R-99-42

SR 97 – Alternative models project

Stochastic continuum modelling of Aberg

Hans Widén
Kemakta AB

Douglas Walker
INTERA KB/DE&S

August 1999

Svensk Kärnbränslehantering AB
Swedish Nuclear Fuel
and Waste Management Co
Box 5864
SE-102 40 Stockholm Sweden
Tel 08-459 84 00
+46 8 459 84 00
Fax 08-661 57 19
+46 8 661 57 19

ISSN 1402-3091
SKB Rapport R-99-42

SR 97 – Alternative models project

Stochastic continuum modelling of Aberg

Hans Widén
Kemakta AB

Douglas Walker
INTERA KB/DE&S

August 1999

Keywords: Performance Assessment, Radionuclide Transport, Pathways Analysis, Fracture Flow, Near-Field, Far-Field, FARF31, COMP23, FracMan, PA Works.

ABSTRACT

As part of studies into the siting of a deep repository for nuclear waste, Swedish Nuclear Fuel and Waste Management Company (SKB) has commissioned the Alternative Models Project (AMP). The AMP is a comparison of three alternative modelling approaches to bedrock performance assessment for a single hypothetical repository, arbitrarily named Aberg. The Aberg repository will adopt input parameters from the Äspö Hard Rock Laboratory in southern Sweden. The models are restricted to an explicit domain, boundary conditions and canister location to facilitate the comparison. The boundary conditions are based on the regional groundwater model of Svensson (1997), provided in digital format.

This study is the application of HYDRASTAR, a stochastic continuum groundwater flow and transport-modelling program. The study uses 34 realisations of 945 canister locations in the hypothetical repository to evaluate the uncertainty of the advective travel time, canister flux (Darcy velocity at a canister) and F-ratio. Several comparisons of variability are constructed between individual canister locations and individual realisations. For the ensemble of all realisations with all canister locations, the study found a median travel time of 27 years, a median canister flux of 7.1×10^{-4} m/yr and a median F-ratio of 3.3×10^{5} yr/m. The overall pattern of regional flow is preserved in the site-scale model, as is reflected in flow paths and exit locations. The site-scale model slightly over-predicts the boundary fluxes from the single realisation of the regional model. The explicitly prescribed domain was seen to be slightly restrictive, with 6% of the stream tubes failing to exit the upper surface of the model. Sensitivity analysis and calibration are suggested as possible extensions of the modelling study.

SAMMANFATTNING

Som en del av platsvalsprocessen för ett djupförvar för radioaktivt avfall har Svensk Kärnbränslehantering AB (SKB) beställt ett projekt med jämförelse av alternativa modeller (AMP - Alternative Models Project). AMP är en jämförelse av tre alternativa modellprinciper för säkerhetsanalys av berggrunden, alla för samma hypotetiska modellområde. Det hypotetiska modellområdet, kallat Aberg, antar värden på indata från Äspö Laboratoriet i södra Sverige. Modellerna är begränsade till ett givet område, givna randvillkor och givna kapselpositioner för att möjliggöra jämförelsen. Randvillkoren baseras på den regionala grundvattenmodellen (Svensson, 1997), tillhandahållna i digitalt format.

Denna studie är appliceringen med HYDRASTAR, en stokastisk kontinuum grundvattenflödes och transportmodell. I studien har 34 realiseringar av de 945 kapselpositionerna, från ett tänkt förvar, använts för att bedöma osäkerheter i gångtid, flödestäthet vid kapsel och F-faktorn. Flera jämförelser av variationer görs mellan individuella kapslar och individuella realisationer. För alla kapslar och alla realisationer, erhölls följande medianvärden: vattengångtid 27 år, flödestäthet vid kapsel 7.1 x 10^{-4} m/år och F-faktor 3.3 x 10^{5} år/m. Det totala mönstret för det regionala flödet bevaras i modellen över lokalområdet, vilket återspeglas i flödesvägar och slutpunkter. Lokalmodellen tenderar att ge lite högre flöden vid ränderna jämfört med den enskilda realisationen för regionalmodellen. Det förutbestämda modellområdet visade sig vara något för litet, eftersom 6% av partiklarna inte nådde ytan inom modellområdet. Känslighetsanalys och kalibrering föreslås som möjliga utvidgningar av studien.

TABLE OF CONTENTS

LIST OF FIGURES

LIST OF TABLES

EXECUTIVE SUMMARY

The Alternative Models Project (AMP) is part of the SKB SR 97 study, and consists of a comparison of three alternative modelling approaches to bedrock performance assessment (PA) at the Aberg site. This study is an application of HYDRASTAR, a stochastic continuum groundwater flow and transport modelling program. Flow in the host rock is modelled via Darcy's Law, using unconditional geostatistical simulation to create multiple realisations of the hydraulic conductivity field. The application is relatively straightforward, with the majority of the model parameters and boundary conditions explicitly specified by SKB in the project requirements memo by Ström and Selroos (1997). The parameters are unchanged from those given in Ström and Selroos (1997), except that the hydraulic conductivities are adjusted as suggested by Svensson (1997) and rescaled as suggested by Walker et al. (1997). The SKB geostatistical analysis code INFERENS is used to infer a regularised variogram model, based on the 3m interpreted hydraulic conductivities taken from SICADA.

The boundary conditions for this model are constant head boundaries, derived from a single stochastic realisation of a regional scale model by Svensson (1997). The overall flow pattern is that of recharge on the inland areas discharging to the coastal waters. The transfer of regional heads via constant head boundaries preserves this pattern in the site-scale model. The median boundary flux across the site-scale domain is slightly greater than that of the single realisation of the regional model. However, the single realisation of the regional model might not represent the expected boundary conditions, which limits the applicability of the fine-tuning of rescaling with respect to mass balance.

The study uses 34 realisations of 945 canister locations to evaluate three performance measures for the proposed repository: the travel times, canister fluxes, and F-ratios. Two realisations are examined in detail to illustrate the variability within individual realisations. The individual realisations are selected as being typical with respect to travel time and canister flux. Because the porosity is homogeneous in the model, the travel times and canister fluxes are inversely correlated. Consequently, although one realisation is selected based on the travel time and another based on the canister flux, the realisations are quite similar. Three individual canister locations, one from each of the three repository blocks, are examined over all 34 realisations to illustrate uncertainty in estimates and differences due to location. All three have approximately the same median $\log_{10}$ travel times and F-ratios, but the median $\log_{10}$ canister fluxes differ, as do their distributions.

The results of the variability between realisations (i.e., statistics of each realisation, compared among the 34 realisations) are somewhat unclear because of the low number of realisations. The variability of the means, medians and variances appears to be quite low between realisations.

However, the histograms of these statistics are ambiguous because of the limited number of realisations.

The ensemble results taken over all statistics for all canister locations suggest a median travel time of 27 years, a median canister flux of 7.1×10^{-4} m/yr and a median F-ratio of 3.3×10^{5} yr/m.

The current version of HYDRASTAR is limited to homogeneous flow porosity over the entire domain, so that the F-ratio is a multiple of the travel time. The $\log_{10}$ travel time and $\log_{10}$ canister flux distributions essentially are symmetric. The flow paths and exit locations of the realisations are compatible with the overall pattern of flow at the site. The explicitly prescribed domain is seen to be slightly restrictive, with 6% of the stream tubes failing to reach the upper surface of the model. In several respects, the modelling could be improved within the current features of HYDRASTAR. These include extending the domain, sensitivity analysis and calibration. Other improvements, such as explicit modelling of salinity, lie outside of the abilities of the current version of HYDRASTAR.

1. INTRODUCTION

1.1. THE ALTERNATIVE MODELS PROJECT

Swedish Nuclear Fuel and Waste Management Company (SKB) is responsible for the safe handling and disposal of nuclear wastes in Sweden. This responsibility includes conducting studies into the siting of a deep repository for high-level nuclear waste. The Safety Report 1997 (SR 97) will present a comparative performance assessment (PA) of the long-term safety of three hypothetical repositories in Sweden. This will include hydrogeologic modelling to examine the possible transport of radionuclides from the emplaced waste packages through the host rock to the accessible environment. One important subtask of SR 97 is the Alternative Models Project (AMP), which is a comparison of three alternative modelling approaches to bedrock PA.

The overall goal of the AMP is to illustrate the consequences of the three primary alternative modelling approaches to PA used by SKB. These are the stochastic continuum (SC), discrete feature network (DFN), and channel network (CN) approaches to groundwater flow and transport modelling. The AMP applies these different conceptual models to the safety assessment of a single hypothetical repository for high-level wastes. The stated objectives of the AMP are:

- to illustrate the rock barrier performance using different conceptual models for groundwater flow and mass transport in fractured rocks
- to show the robustness of the assessment model in terms of relevant far field performance measures.

The emphasis of the AMP is that the results of the three approaches should be as comparable as possible. To help achieve this goal, Ström and Selroos (1997) have described the specific project requirements of the AMP. The hypothetical repository, arbitrarily named Aberg, adopts input parameters from the Äspö Hard Rock Laboratory in southern Sweden, a site previously investigated by SKB. Rhén et al. (1997) and Walker et al. (1997) document the data. The models are restricted to an explicit domain, boundary conditions and canister locations. The boundary conditions are based on the regional groundwater model of Svensson (1997), provided in digital format.

1.2. STUDY OVERVIEW

This report summarises the AMP study of the stochastic continuum (SC) modelling approach to bedrock performance assessment. The study utilises the SKB groundwater modelling program, HYDRASTAR, a finite difference groundwater flow modelling program. The tasks involved in this effort include the interpretation of the hydrogeologic model into HYDRASTAR format, upscaling of covariance models, simulation and sensitivity analysis, interpretation and illustration of results, and summary reporting. A minor programming task is also required to interpret the hydraulic heads of the regional model to boundary conditions suitable for HYDRASTAR input.

2. MODELLING APPROACH

2.1. THE PA MODEL CHAIN

HYDRASTAR – COMP23 –FARF31 is the geosphere portion of the performance assessment model chain developed during the 1990's by SKB for use as a computational tool in the 1995 SKB safety analysis project (SR 95). Figure 2-1 illustrates the PA model chain, whose end product is the calculation of the probable radionuclide flux to the biosphere. The hydrology model is HYDRASTAR, which is used to determine the Darcy groundwater flux at the canister locations (canister flux) and the advective travel paths (stream tubes) through the geosphere. COMP23 is the near-field model, which uses the canister fluxes to determine the release rate for radionuclides from the emplaced canisters and into the groundwater flow system. FARF31 uses both the release rates from the canisters and the stream tubes through the groundwater flow system to determine the probable radionuclide flux to the biosphere. (SKB, 1996). Note that this report discusses only the HYDRASTAR portion of the model chain.

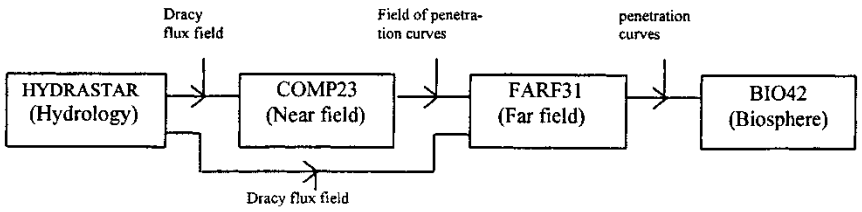

Figure 2-1. *SKB SR 95 PA Model chain.*

2.2. HYDRASTAR

HYDRASTAR is a stochastic groundwater flow and transport modelling program developed as a quantitative tool for support of the SKB 91 safety analysis project (SKB, 1992). A flow chart summarising the HYDRASTAR algorithm is presented in Figure 2-2. The current version, 1.7, uses the Turning Bands algorithm (Journel and Huijbregts, 1978) to generate realisations of the hydraulic conductivity field conditioned on the observed hydraulic conductivities. Trends in the data may be included implicitly through the use of ordinary kriging neighbourhoods or prescribed explicitly for specific regions. Hydraulic conductivity measurements at the borehole scale are upscaled to the model calculation scale using a regularisation scheme based on Moye's formula (a corrected arithmetic mean of the packer test hydraulic conductivities within a block; see Norman, 1992b, for details). HYDRASTAR uses the governing equation for either time-dependent or steady state groundwater flow in three dimensions, assuming constant density. The solution to this governing equation is approximated by a node centred finite-difference method to create a linear system of equations. A pre-conditioned conjugate-gradient algorithm solves the system of equations to arrive at a solution for the hydraulic head at each node. The pilot point inverse method (de Marsily et al., 1984) can be used to calibrate the input hydraulic conductivity field to minimise the error between the simulated and observed hydraulic heads. Transport in the resulting velocity field is modelled as pure advection using a particle tracking scheme to determine the stream tubes (flow paths) from each starting location. The process of conditional geostatistical simulation of hydraulic conductivity, calibration of the field via inverse modelling, and particle tracking can be repeated in Monte Carlo fashion to develop empirical probability distributions for the hydraulic conductivity field, and the travel paths and arrival times for advected contaminants.

Starprog AB developed and tested the code under contract to SKB, beginning in 1991 (Norman 1991 and 1992b). Various authors have contributed to the development and testing of the code, most notably Norman (1991 and 1992b), Morris and Cliffe (1994), Lovius and Eriksson (1993, 1994), Walker et al. (1997) and Walker (1997). The test problems include comparisons to well-known analytical and numerical solutions, or are taken from the HYDROCOIN series of test problems (OECD, 1983; Hodgkinson and Barker, 1985). The code also has been applied successfully to the Finnsjön site, as part of the SKB 91 Project (Norman, 1992a and SKB 1992).

This application does not use all the available features in the current version of HYDRASTAR. Conditional geostatistical simulation using borehole data is not used (i.e., the hydraulic conductivity fields are created via unconditional geostatistical simulation), nor are pilot point calibration or transient simulation. The Moye's formula upscaling of borehole data is only used as part of INFERENS analysis of the data to infer a variogram model. Trends in the hydraulic conductivity are included only as discrete, stepwise changes to represent fracture zones, rock units (i.e., no continuous decrease with depth is used).

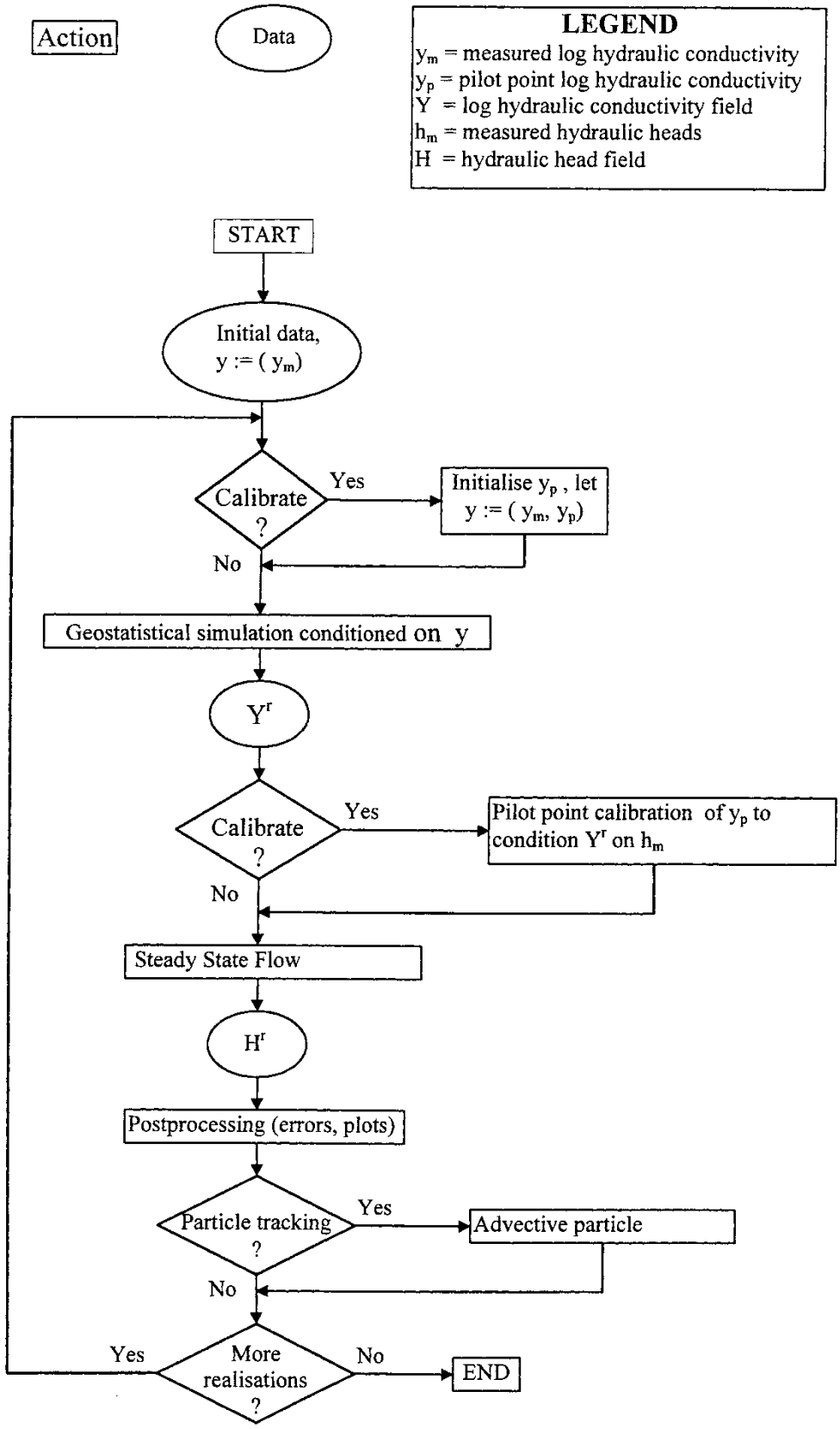

Figure 2-2. *HYDRASTAR flow chart.*

3. MODEL APPLICATION

Ström and Selroos (1997) explicitly specify the extent and boundary conditions for the model domain, the geologic structures, the canister locations, the hydraulic conductivities, and the transmissivities to be used for the AMP studies. Ström and Selroos (1997) also indicated that interpreted hydraulic conductivities for site borehole hydraulic tests could be taken from SICADA. In addition to these parameters, HYDRASTAR also requires a geostatistical description of the hydraulic conductivity that is appropriate for the grid scale of interest. Walker et al. (1997) explores and infers a geostatistical model for the hydraulic conductivity, resulting in adjustments of the hydraulic conductivity values provided in the memo (see Section 3.5).

3.1. SITE DESCRIPTION

Aberg takes its data from the Äspö site, which is located in southern Sweden, in the northern part of Småland (Figure 3-1). It is just off the Swedish coast in the Baltic Sea, near Oskarshamn nuclear power plant. The Äspö site is also the location of the Äspö Hard Rock Laboratory (HRL), an underground research facility owned and operated by SKB. From a hydrogeologic perspective, the region is notable for the low topographic relief, intrusion of saltwater from the Baltic Sea and the fracturing associated with the Äspö shear zone.

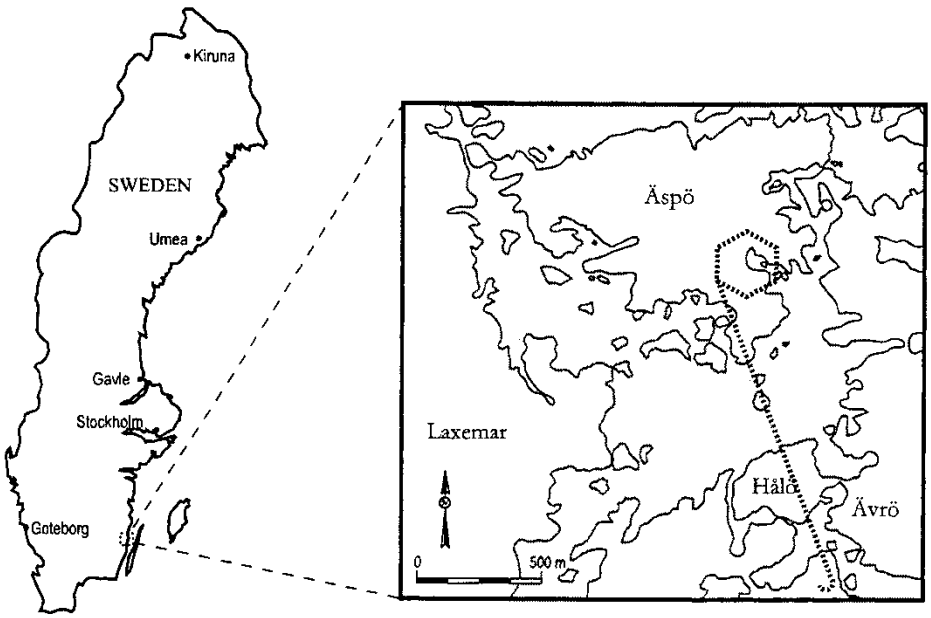

Figure 3-1. Location of the Äspö site and Hard Rock Laboratory.

3.2. HYDROGEOLOGY

The geology and hydrogeology of the Äspö site has been studied in great detail and are summarised in a series of reports (Wikberg et al., 1991; Rhén et al., 1997). Walker et al. (1997) presents a summary of site conditions emphasising continuum modelling.

Äspö regional geology consists of a crystalline bedrock dominated by the heterogeneous Småland granite suite. The Äspö shear zone, running SW-NE through Äspö Island divides the bedrock into two parts. The region continues to experience isostatic rebound as a consequence of the last period of continental glaciation. This glaciation also deposited bouldery till throughout the region. Peatlands are found in some depressions, as are fluvial sand and gravel. The soil cover is thin with numerous bedrock outcrops. Regional lineaments have been mapped and examined by various airphoto, aerogeophysical, outcrop, seismic and borehole studies, revealing a number of major discontinuities that have been interpreted as steeply dipping fracture zones. The salinity profile of the groundwater system is typical of islands and coastal areas: fresh groundwater near the surface rests on saline water that has intruded from the sea.

The hydrology of the area around and on Äspö was compiled during 1986-1987. Precipitation generally exceeds evapotranspiration resulting in a small net recharge on the land surface. The classical model of topographic drive suggests that recharge will occur in higher elevations and flow to discharge areas in lower elevations. This should be combined conceptually with the classical model of seawater intrusion under freshwater in coastal areas and islands. Although simplistic, this general model is consistent with the locations of streams, mires, observed hydraulic heads, salinity distributions and geochemical data available in the region. Svensson (1995, 1997) used a groundwater flow model to demonstrate that the overall pattern of groundwater flow at depth can be explained by this combination of conceptual models.

3.3. REGIONAL MODEL AND BOUNDARY CONDITIONS

Ström and Selroos (1997) specified that all three models in the AMP study use an explicit site-scale domain defined as a volume 2000m by 2000m of horizontal extent, 1000m in depth (Figure 3-2). The upper surface of the model is given at sea level (0 masl). All of the AMP models are to rely on boundary conditions derived from the regional groundwater flow modelling study of Svensson (1997). That study used a finite difference continuum model, PHOENICS, to study ground water recharge and regional flow patterns. The results of that study included the steady state heads and fluxes along the limits of the site-scale model domain. Ström and Selroos (1997) specified that these head values should be used as constant head (Dirichlet) boundary conditions by all three of the AMP studies.

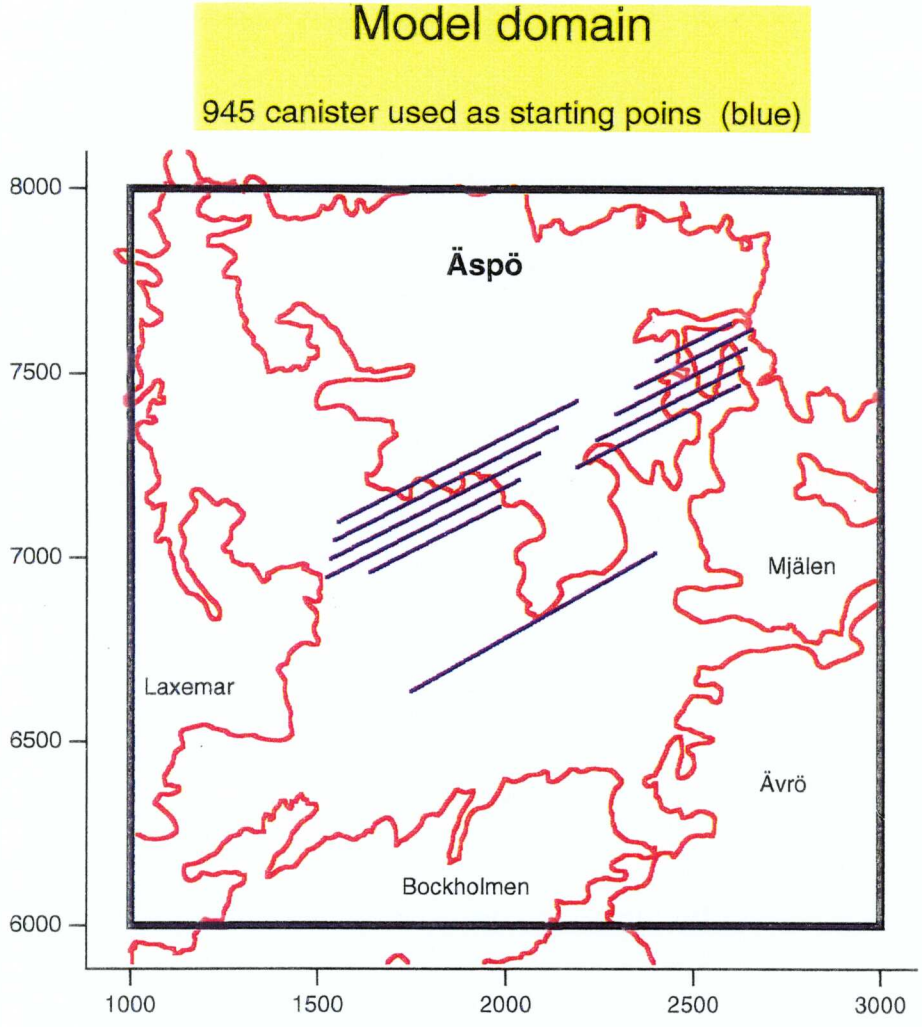

Figure 3-2. *Äspö site and AMP domain. Waste canister locations shown in blue.*

These head values require some adaptation for use in the smaller scale HYDRASTAR model. The head values provided by Svensson (1997) are given on 100m grid spacing, and must be interpolated to the HYDRASTAR grid spacing of 25m. This was accomplished using a MATLAB program for 2-dimensional linear interpolation to create a set of head values on each model surface. The output of this MATLAB program was written to a file in the same format as that used by the HYPAC code TBCSTA, which normally is used to transfer boundary conditions from NAMMU to HYDRASTAR. This allows the interpolated heads to be transferred to HYDRASTAR as a Dirichlet boundary using the NAMMU option in HYDRASTAR.

This interpolation of heads matches the site-scale boundary heads to the regional scale heads for the same domain (i.e., conservation of energy). Although this approach is the same as used in other nested groundwater models (e.g., Ward et al., 1987), it is also important to verify that the fluxes across the boundary are the same (i.e., conservation of mass). The consistency of the boundary fluxes is discussed further in section 4.0.

3.4. MODEL LAYOUT

Ström and Selroos (1997) specified the location and extent of the site scale domain for the AMP studies. The HYDRASTAR model for this application consists of a 3-dimensional finite difference grid with a uniform grid spacing of 25m. The resulting grid of 81 by 81 by 41 nodes (width, length and depth, respectively) gives a typical size for HYDRASTAR models that can be run on the SKB CONVEX in the time allotted for this study.

Ström and Selroos (1997) also specify repository layout and canister locations. Figure 3-2 shows these canister locations, which are a modification of layout H from Munier et al. (1997). A total of 945 canister locations are specified and used as starting locations for stream tubes in the HYDRSTAR particle tracking algorithm.

3.5. INPUT PARAMETERS

HYDRASTAR requires input of a structural, hydraulic, and geostatistical description of the site, all at appropriates scales. As prescribed by Ström and Selroos (1997), this study uses the site-scale description derived from the pre-investigation and construction phases summarised in Rhén et al. (1997). Pre-construction investigations and tunnel construction identified a number of fracture zones between 5 to 50m in width. Fractures elsewhere in the site (i.e., those not included in the deterministic zones) are collectively included in the hydraulic conductivity estimates for the rock mass. Consequently, the hydraulic conductivity data is divided into two populations based on the site structural model (Rhén et al., 1997):

- Rock Domain (RD) - borehole tests outside the deterministic hydraulic conductors.
- Conductor Domain (CD) - borehole tests judged to be within the deterministic hydraulic conductors.

Within the site, Rhén et al (1997) divided the rock domain into hydrogeologic units, designated SRD1 through 5. The conductor domain for the site scale (SCD) is divided into units corresponding to mapped hydraulic conductors (e.g., NE-1).

3.5.1. Adjustments to Input Parameters

Ström and Selroos (1997) specified the hydraulic conductivities to be used for each SRD and SCD, which were based on injection and pumping tests performed in the cored boreholes and tunnel probeholes (Figure 3-3). These tests were interpreted and the measurements reported for various depths, rock types, etc. by Rhén et al. (1997). This HYDRASTAR application uses the values of Ström and Selroos (1997) without modification, except for the rescaling of hydraulic conductivities and the modification of the hydraulic conductivity of SRD4. The hydraulic conductivity of SRD4 is discussed in Section 3.5.3

As discussed in Walker et al. (1997), hydraulic conductivity is a scale-dependent parameter, which requires that the measured hydraulic conductivities be rescaled to the model finite-difference grid scale. The values provided by Ström and Selroos (1997) were taken from Rhén et al. (1997) with an inferred measurement scale of 100m. This application of HYDRASTAR, in contrast, uses a finite difference grid spacing of 25m. This study assumes that the geometric mean of hydraulic conductivity at the measurement scale, L_m, may be adjusted for scale using the regression equation:

$$Log_{10}K_{gu} = Log_{10}K_{gm} + 0.782(Log_{10}L_u - Log_{10}L_m)$$

where:

K_g = geometric mean of hydraulic conductivity (m/s)
L = length scale (m), assumed equal to the packer interval.

The subscripts m and u refer to the measurement and upscaled values, respectively. This empirical scaling relationship was developed by Rhén et al. (1997) using the 3m, 30m, 100m packer tests and full-length tests in the same cored boreholes. This study uses the above relationship to downscale the values given by Ström and Selroos (1997) to determine the mean $\log_{10}$ hydraulic conductivity for simulating K_b, the block-scale conductivities.

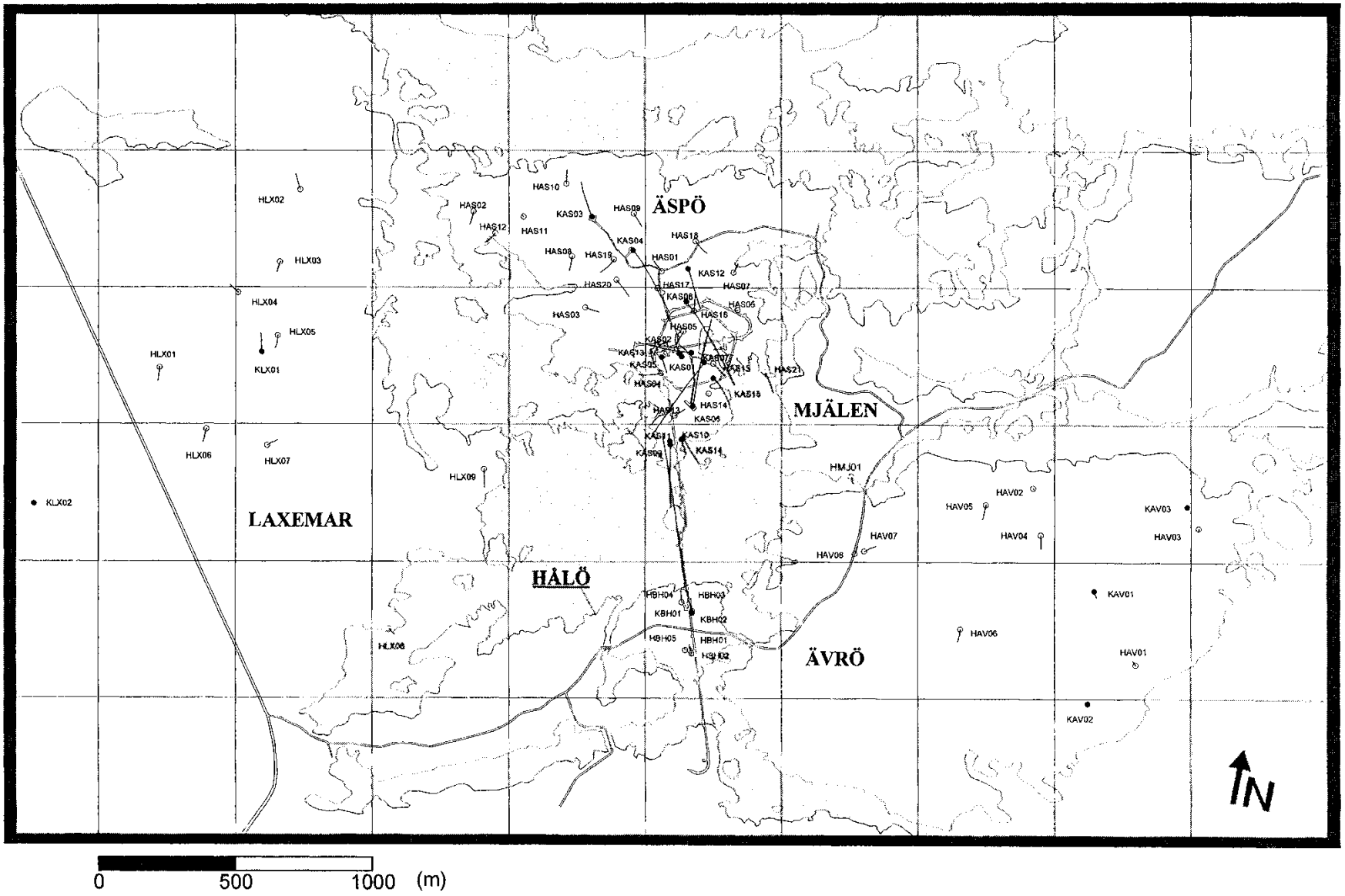

Figure 3-3. *Äspö tunnel and boreholes.*

3.5.2. Conductor Domain (SCD)

The geometries of the hydraulic conductor domains are defined by the major discontinuities described in Rhén et al. (1997). As shown in Figure 3-4, each zone is represented as a planar feature of constant and width, as specified by Ström and Selroos (1997). Note that one deterministic hydraulic conductor, NNW-8, is not shown in Figure 3-4 because it is not thought to reach the surface. Several types of hydraulic tests have been performed in the individual conductive structures, as summarised by Rhén et al. (1997). Note that these tests were on varying measurement scales, thought to be on the order of 50 to 100m (Rhén, personal communication, 1997). This study assumes that the measurement scale is 100m, and that the specified constant transmissivity is an effective transmissivity. This study therefore divides the specified transmissivities by the given widths, and downscales the using the above relationship to reach block scale conductivities for use in HYDRASTAR The resulting values are provided below in Table 3-1.

Table 3-1. Aberg site-scale conductors (SCD1). 100m measurements from Rhén et al. (1997), scaled to 25m.

Zone	Median Log_{10} K (m/s)		Width (m)	Sample size
	100m	25m		
EW-1N	-7,30	-7,79	30	4
EW-1S	-6,13	-6,62	30	4
EW-3	-5,80	-6,28	15	4
EW-7	-5,17	-5,65	10	3
NE-1	-5,00	-5,48	30	16
NE-2	-7,09	-7,57	5	12
NE-3	-5,24	-5,72	50	9
NE-4	-6,12	-6,61	40	8
NNW-1	-6,26	-6,74	20	7
NNW-2	-5,55	-6,04	20	4
NNW-3	-6,00	-6.50	20	0
NNW-4	-4,82	-5,31	10	8
NNW-5	-7,00	-7,48	20	3
NNW-6	-6,00	-6.60	20	0
NNW-7	-6,62	-7,10	20	5
NNW-8	-6,30	-6,79	20	3
NW-1	-7,77	-8,25	10	3
SFZ11	-6.30	-6.80	20	0
SFZ14a,b	-6,30	-6.80	20	0

All fracture zones that are less than 30 metres wide are modelled as 30m. The conductivities of such zones are adjusted so that the zones will have the same transmissivity as given in Table 3-1.

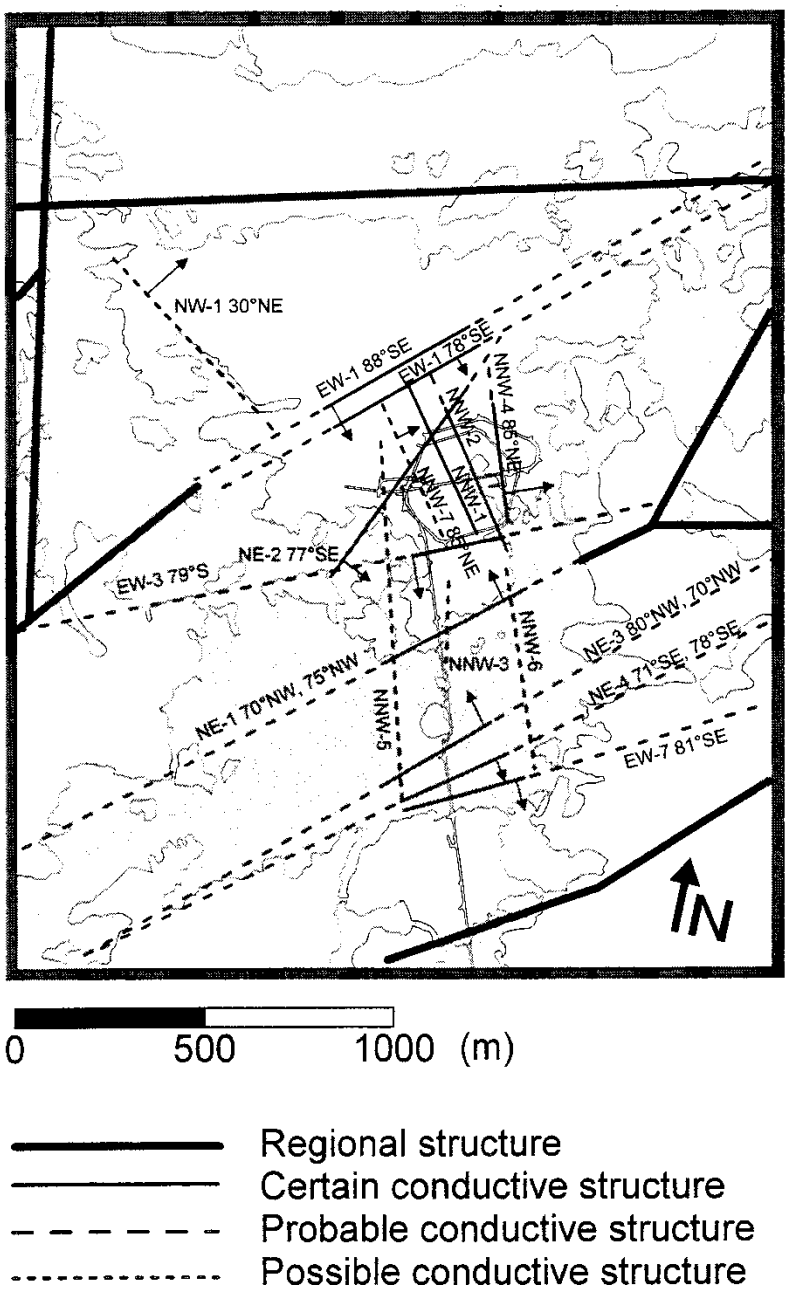

Figure 3-4. *Äspö site-scale conductor domains.*

3.5.3. Rock Domain (SRD)

Based on observations taken during the pre-investigation and construction of the Äspö HRL, the Äspö site is divided into five site rock mass domains (SRD; Rhén et al. 1997; see also Figure 3-5). The mean $\log_{10}$ hydraulic conductivities for domains SRD1-3 are based on the interpreted hydraulic conductivities of the 3m packer tests. The areas outside the SRD's but inside the model domain are assigned the mean of all the 3m interpreted $\log_{10}$ hydraulic conductivities. As with the conductor domains, these values must be upscaled from 3m measurement scale to a 25m finite difference grid scale. Table 3-2 presents the upscaled values used in this study.

The mean $\log_{10}$ hydraulic conductivity of SRD4 (southern Äspö, south of NE-1) requires special consideration. There are no 3m hydraulic tests within SRD4, thus Rhén et al. (1997) inferred hydraulic properties for SRD4 based on hydraulic tests in the tunnel probeholes. Rhén et al. (1997) suggested a mean $\log_{10}$ hydraulic conductivity of –6.26 at the 100m scale, as specified by Ström and Selroos (1997). Based on calibration of a numerical model to observed drawdowns, Svensson has suggested that the geometric mean hydraulic conductivity of SRD4 be reduced to –7.6 (at a 20m finite difference block scale). This value is thought to best represent the properties of SRD4 and the drawdowns observed during construction and testing of the HRL (Svensson, personal communication, 1997; Rhén, personal communication, 1997). Consequently, this study will use the calibrated values of Svensson for SRD4 instead of the value specified by Ström and Selroos (1997).

Note that the SRD descriptions of Rhén et al. (1997) extended to a depth of 600mbgs, beneath which is a zone of lower hydraulic conductivity. For the purposes of this study, this lower zone was omitted and the SRD zones were continued to the bottom of the modelled domain Also note that most of the repository specified by Ström and Selroos (1997) lies in SRD3, which has a relatively low hydraulic conductivity. Consequences of this layout are discussed further in Section 5.0.

Table 3-2. Aberg site-scale rock mass (SRD). 3m measurements from Rhén et al. (1997), scaled to 25m.

SRD	Log_{10}K (m/s)	
	3m	25m
SRD1	-8.74	-8.0
SRD2	-7.82	-7.1
SRD3	-9.47	-8.8
SRD4 *	-7.6*	-7.5
SRD5	-8.32	-7.6
Other (aver SRD1 - 3)	-9.26	-8.5

* Based on calibration of 20m numerical model by Svensson, 1997

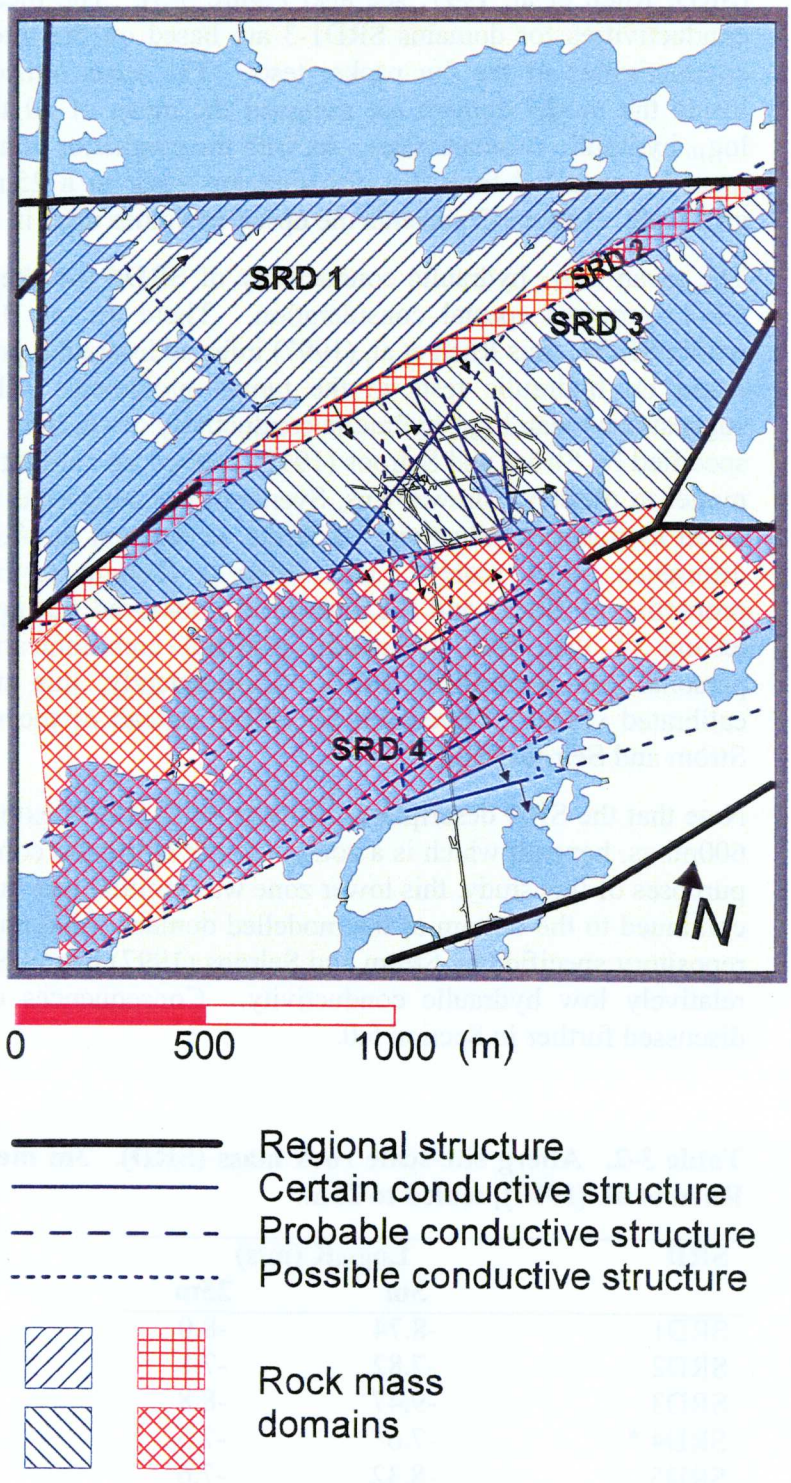

Figure 3-5. *Äspö site-scale rock domains (SRD).*

3.5.4. Geostatistical model

The Aberg site-scale geostatistical model of hydraulic conductivity consists of the rock blocks described for SRD1 through 5, the SCD and a single variogram model. The variogram model is inferred via geostatistical analysis of the interpreted hydraulic conductivities from the single hole hydraulic tests. The interpreted hydraulic conductivities for the 3m packer tests were taken directly from the SKB SICADA database, and analysed with INFERENS, the SKB geostatistical analysis and inference program.

HYDRASTAR's geostatistical simulation algorithm is limited to a single variogram model for both domains. Because the SRD data is more abundant, this study infers a regularised variogram model based on only the test data in the rock domain for both the SRD and SCD (Walker et al., 1997). Unlike previous geostatistical studies of the Äspö data (LaPointe, 1994; Winberg, 1994; Niemi, 1995), this study uses the Rhén et al. (1997) interpreted hydraulic conductivities for the 3m packer tests. This is important because the Rhén interpretation has no lower measurement limit, a characteristic that can effect the statistics of the data.

As is discussed in Walker et al. (1997), the variogram must be adjusted (regularised) to account for the difference between measurement and grid scales. The interpreted conductivities are taken from cored boreholes KLX01, KAS02, KAS03, KAS04, KAS05, KAS06, KAS07 and KAS08, as found in SICADA. The SKB code INFERENS was used to upscale the 3m data to 25m and fit a model variogram to the rock mass data (Walker et al., 1997). Results of this analysis indicated the following variogram model for the 25m grid scale (Figure 3-6):

- Exponential model, isotropic
- practical range of 97 m
- zero nugget, variance 2.72

The SRD and SCD are treated as step changes in the geometric mean of block conductivities (0 order trends in K_b), with values provided in Tables 3-1 and 3-2. The fields are simulated unconditionally, i.e., without direct use of the hydraulic conductivity measurements. Figure 3-7 shows the HYDRASTAR representation of the SCD and SRD within the model domain. Figure 3-8 is a plot of a single realisation (number 1) of the unconditional $\log_{10} K$ field, on the plane cutting through the repository (z = -500 masl.

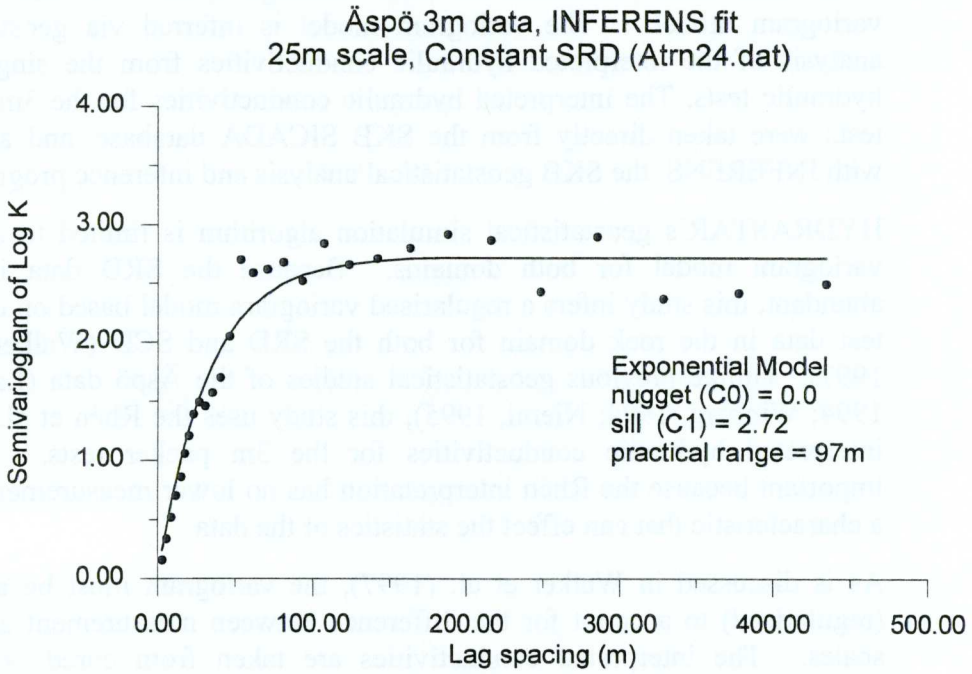

Figure 3-6. *Semivariogram of log_{10} of hydraulic conductivity for 25m scale.*

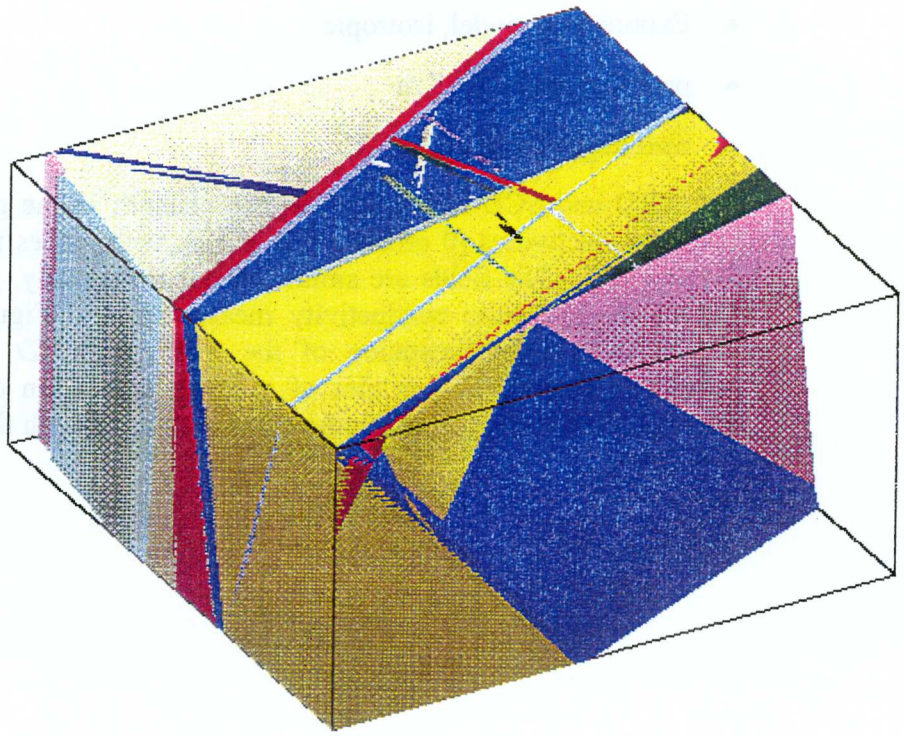

Figure 3-7. *HYDRASTAR Representation of SCD and SRD within model domain. (The colours do not correspond to hydraulic property).*

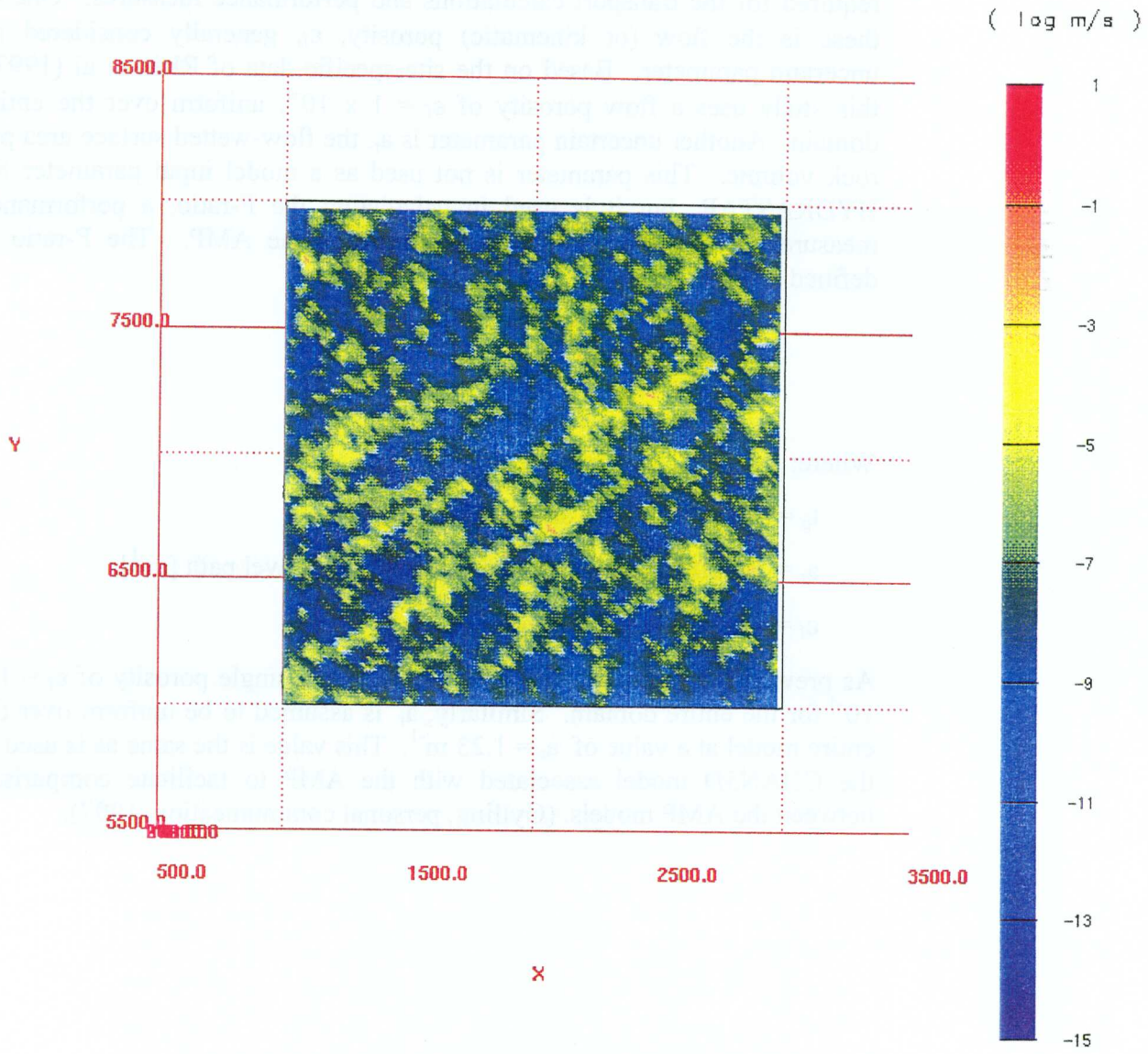

Figure 3-8. *Log_{10} of hydraulic conductivity on a plane cutting through repository level (z = -500 masl), realisation number 1.*

3.5.5. Other parameters

The remaining HYDRASTAR input parameters are hydraulic parameters required for the transport calculations and performance measures. One of these is the flow (or kinematic) porosity, ε_f, generally considered an uncertain parameter. Based on the site-specific data of Rhén et al (1997), this study uses a flow porosity of $\varepsilon_f = 1 \times 10^{-4}$, uniform over the entire domain. Another uncertain parameter is a_r, the flow-wetted surface area per rock volume. This parameter is not used as a model input parameter for HYDRASTAR, but it is used in calculating the F-ratio, a performance measure used in comparing model results in the AMP. The F-ratio is defined as:

$$F_p = \frac{t_p a_r}{\varepsilon_f}$$

Where:

t_p = travel time in a stream tube [years]

a_r = specific surface per rock volume for a travel path [m^{-1}]

ε_f = flow (kinematic) porosity [.]

As previously mentioned, HYDRASTAR uses a single porosity of $\varepsilon_f = 1 \times 10^{-4}$ for the entire domain. Similarly, a_r is assumed to be uniform over the entire model at a value of $a_r = 1.23\ m^{-1}$. This value is the same as is used in the CHAN3D model associated with the AMP to facilitate comparison between the AMP models. (Gylling, personal communication, 1997).

4. SIMULATIONS

Model simulations are conducted on SKB's Convex 220, and the results are summarised using the commercial software packages STATISTICA, MATLAB and AVS. For each simulation, HYDRASTAR creates a new unconditional simulation of the hydraulic conductivity field. Steady-state groundwater flow is simulated in each realisation to determine the Darcy groundwater velocity at each canister location (the canister flux) and the spatially variable velocity field. These fluxes and the velocity field are used to determine the stream tubes (flow paths) and travel times using advective particle tracking. Starting points for each stream tube correspond to the 945 canister locations specified by Ström and Selroos (1997; see also Figure 3-2).

4.1. MONTE CARLO SIMULATION STABILITY

A practical consideration in Monte Carlo simulation studies is that the estimated distribution of model results be stable with respect to the number of realisations. That is, the number of realisations should be adequate for reliable estimates of the model uncertainty. Figures 4-1 and 4-2 present the medians of the logarithm of travel time and the logarithm of canister flux, respectively, versus the number of realisations. The plots indicate these statistics are approximately constant after 20 realisations, with less than 5% deviation for additional realisations. To be sure that the statistics would remain stable, a few additional realisations were performed for a total number of 34 realisations.

The stability of the median and arithmetic mean should not be taken to imply that higher moments such as the variance are also stable. Estimators of higher moments and the extreme quantiles of distributions are usually much less efficient than the median or the mean (Larsen and Marx, 1986). In general, estimating these moments with a similar degree of accuracy requires many more realisations than are needed for stable estimators of the median (Hammersley and Handscomb, 1975). Consequently, the higher-order performance measures of Section 5 may not have stabilised and should be used cautiously.

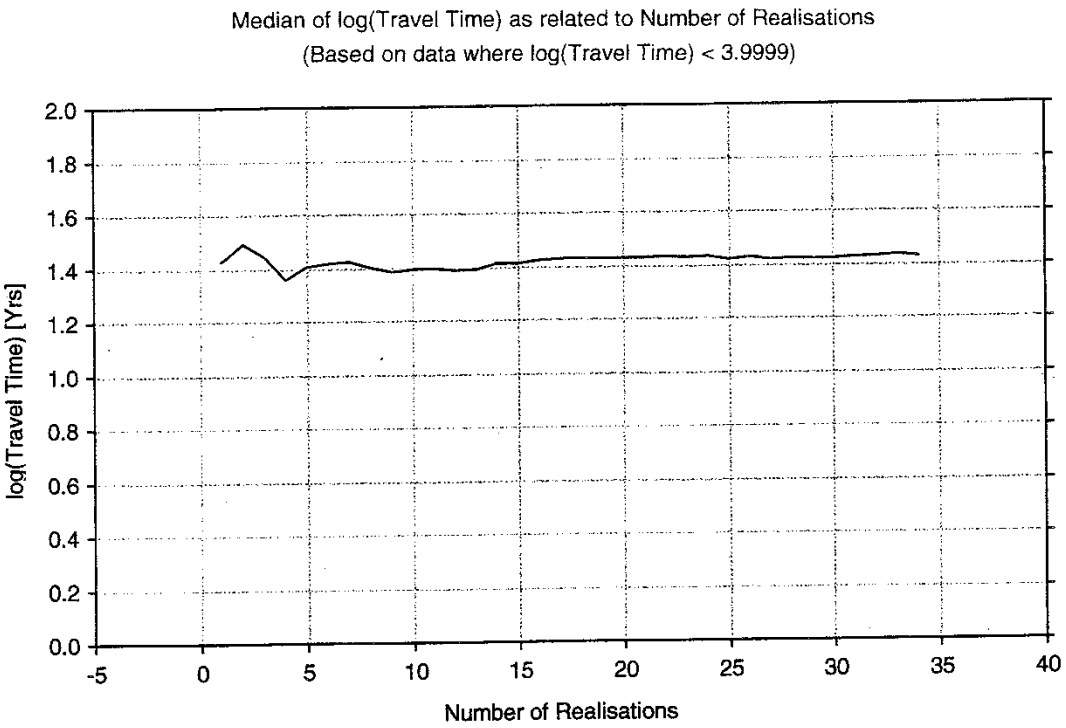

Figure 4-1. *Monte Carlo stability: Median travel time versus number of realisations for travel times less than 10000 years.*

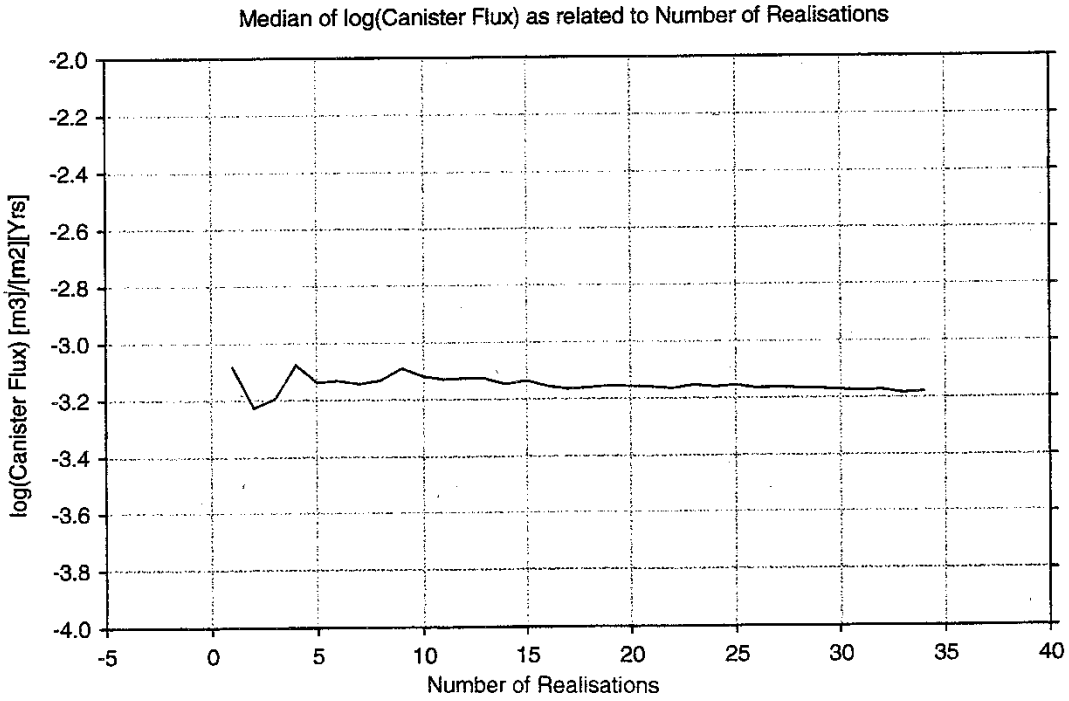

Figure 4-2. *Monte Carlo stability: Median canister flux versus number of realisations for travel times less than 10000 years.*

4.2. CONSISTENCY OF BOUNDARY FLUXES

Stochastic continuum theory suggests that, under certain conditions, there exists an effective hydraulic conductivity, K_e, that satisfies:

$$\langle \bar{q} \rangle = -K_e \nabla \langle \bar{h} \rangle$$

Where:

$\langle \bar{q} \rangle$ = the expected flux over the domain

$\nabla \langle \bar{h} \rangle$ = the expected gradient

(Dagan, 1986). K_e is useful for nested models in that it can be used to estimate the expected value of the flux in a smaller domain (Rubin and Gómez-Hernández, 1990). This suggests that a regional model with a homogeneous hydraulic conductivity of K_e could be used to determine the expected boundary fluxes of a site-scale model subdomain. If the rescaling of the geometric mean hydraulic conductivity is correct, the expected boundary flux should be consistent with the average boundary flux of the site-scale stochastic continuum model. That is, the site-scale stochastic continuum model should conserve mass in an average sense with respect to the regional model fluxes.

However, the model of Svensson (1997) did not use a homogeneous hydraulic conductivity for the regional model. Instead, Svensson created a single stochastic realisation of heterogeneous hydraulic conductivities. The block conductivities were simulated assuming a lognormal distribution, no spatial correlation and the 100m scale K values as the geometric mean of block hydraulic conductivity. That is, the boundary fluxes specified by Ström and Selroos (1997) were determined using a single realisation of a heterogeneous model. It is not known how the subdomain boundary fluxes of this heterogeneous field are related to the expected flux of stochastic continuum theory. Therefore, the rescaling of hydraulic conductivities inherent in the stochastic continuum approach to groundwater modelling will not necessarily have the desired average conservation of mass. The comparisons presented in Figure 4-3 and Table 4-1 are presented for discussion purposes only.

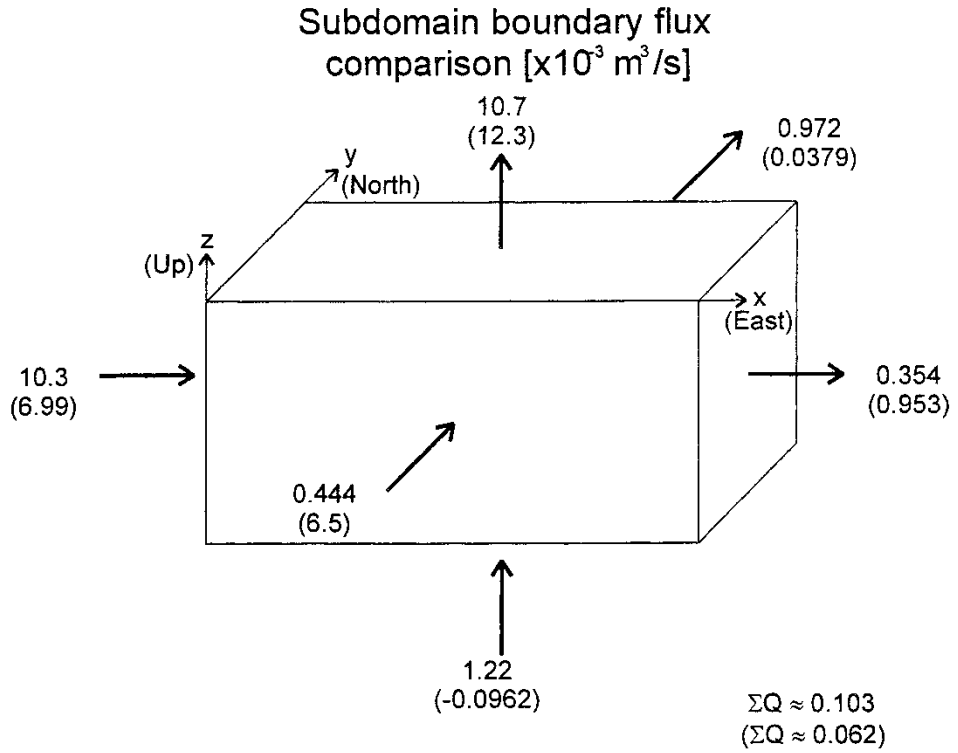

Figure 4-3. *Consistency of Boundary Flux, regional versus site-scale models. Fluxes calculated as the average of 34 realisations of the HYDRASTAR model are given in parentheses.*

As shown in Figure 4-3, both models indicate that the majority of the inflow to the domain comes from the west, and the majority of the outflow is directed out the upper surface of the model to the Baltic Sea. This is consistent with the regional pattern of recharge and discharge. Table 4-1 summarises the fluxes in the x, y, z directions (North, East, and upward in the Äspö coordinate system). The fluxes for the HYDRASTAR site-scale model are the median values for 34 realisations.

It might be possible to modify the geometric means of hydraulic conductivity specified for the SRD to attempt to match the boundary fluxes. However, because the regional model does not necessarily represent the expected flow field as discussed above, there is little sense in trying to match the boundary fluxes as suggested in Walker et al. (1997). In addition, the HYDRASTAR boundary flux output carries only three significant digits, limiting the accuracy of the values in Table 4-1 (Lovius, personal communication, 1998). Any further attempt to adjust the model parameters is consequently not pursued.

Table 4-1 Boundary flux consistency, site-scale versus regional model.

	Net Flux Through Subdomain ($m^3/s \times 10^3$)	
Model Surface	**Site-scale**	**Regional model**
West	6.99 (in)	10.3 (in)
East	0.953 (out)	0.354 (out)
South	6.5 (in)	0.444 (in)
North	0.0379 (out)	0.972 (out)
Bottom	0.0962 (out)	1.22 (in)
Top	12.3 (out)	10.7 (out)
Total inflow	13.5	12.0
Total outflow	13.4	12.0
Mass balance (In – Out)	0.103	-0.062

5. RESULTS

This section of the report discusses the main results of the HYDRASTAR AMP study in terms of the performance measures and statistics specified by Ström and Selroos (1997). As discussed in Section 4.1, the median travel times and median canister fluxes appear to be stable with respect to the number of simulations and are reasonably consistent with the regional model fluxes. 34 realisations are used to estimate the distribution of travel time and canister fluxes using the 945 starting locations. All statistics are calculated with respect to the common logarithm transforms of the travel times, canister fluxes, and F-ratios to facilitate summary and display. No formal test for the lognormality of these results has been performed or is inferred.

Section 5.1 examines individual realisations to illustrate the variability within a realisation. Section 5.2 examines the results for individual canister locations to illustrate the variability between locations in the repository. Section 5.3 examines variability within and between realisations. The remaining sections examine the ensemble results to assess the overall performance of the bedrock.

5.1. TYPICAL REALISATIONS

There are several strategies that could be used to select several realisations that are in some sense representative of the ensemble. One method is to select a number of realisations at random and examine them to get a sense of their overall behaviour. However, this is precisely the goal of Monte Carlo simulation: to determine the average behaviour of a system using an ensemble of realisations. Another method of selecting a representative realisation is to select fields that have a mean or variance of travel time that is close to that of the ensemble. Yet another method is to consider the mean or variance of the canister flux. This study combines these last two methods by selecting fields that represent both the travel time and the canister flux in terms of the average response and its variability. The study uses the following algorithm to select two representative realisations from the set of 34 realisations:

1. Select three realisations with a median $\log_{10}$ travel time closest to the ensemble median of $\log_{10}$ travel time.
2. From the three realisations of step 1., choose the realisation that has a variance of $\log_{10}$ travel time closest to the median variance of $\log_{10}$ travel time over all realisations.
3. Select three realisations with a median $\log_{10}$ canister flux closest to the median of $\log_{10}$ canister flux over all realisations.

4. From the three realisations of step 3., choose the realisation that has a variance of $\log_{10}$ canister flux closest to the median variance of $\log_{10}$ canister flux over all realisations.

Steps 1 and 2 yield realisation number 5 as being representative with respect to travel time. Steps 3 and 4 yield realisation number 13 as being representative with respect to canister flux. For the sake of discussion, this study examines realisation 1 in somewhat more detail than specified by Ström and Selroos (1997).

Figures 5-1 and 5-2 present the stream tubes in realisation number 5 in plan and elevation views. The stream tubes reflect the overall upward flow pattern at the site, as a result of the regional discharge. The stream tubes also tend to drift to discharge areas under the Baltic as a consequence of the recharge on the land surface. As discussed in the previous sections, this flow pattern is a consequence of the regional flow pattern and the effect of the island hydrology. The exit locations of the entire ensemble are discussed in Section 5.4.3

Table 5-1 presents the summary statistics for realisation numbers 5 and 13 over the set of 945 canister locations. Figures 5-3 and 5-4 present the histograms of travel time, canister flux and F-ratio for both of the selected realisations. The canister flux distributions appear to be bimodal, and may reflect the differences between the mean $\log_{10}$ hydraulic conductivities specified for SRD3 and SRD4. It is initially surprising that the median travel times, canister fluxes and F-ratios do not differ appreciably between realisations 5 and 13, even though different criteria were used to select these realisations. This suggests that travel time and canister flux are correlated. If the median travel times are roughly the same for both realisations, then the median F-ratios will be approximately the same since the F-ratio is a simple multiple of the travel time and a constant (Section 3.5.5). The possibility that travel time and canister flux are correlated is discussed in Section 5.4.2.

As will be discussed in Section 5.4.1, a small percentage of stream tubes fail to exit the upper surface of the model. In such a case, HYDRASTAR sets the travel time to the default maximum of 10000 years. Although the percentage is small, the travel time and F-ratio statistics are effected by this default maximum value. Except as noted, this study calculates the travel time and F-ratio statistics for stream tubes with travel times less than 10000 years. The canister flux is unaffected by the default maximum, and therefore use the full set of stream tubes.

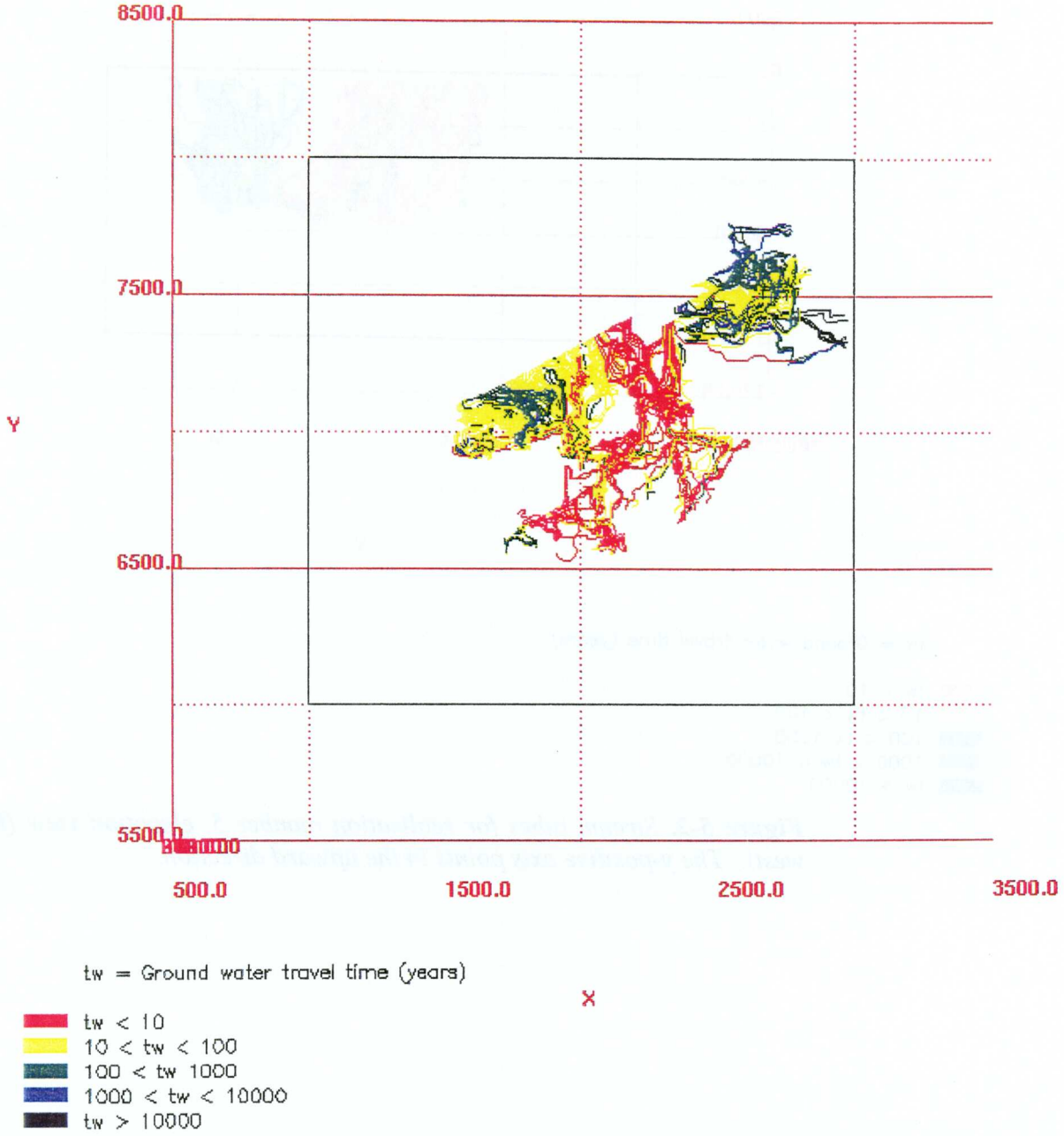

Figure 5-1. *Stream tubes for realisation number 5, plan view (looking downward). The y-positive axis points in the direction of Äspö North.*

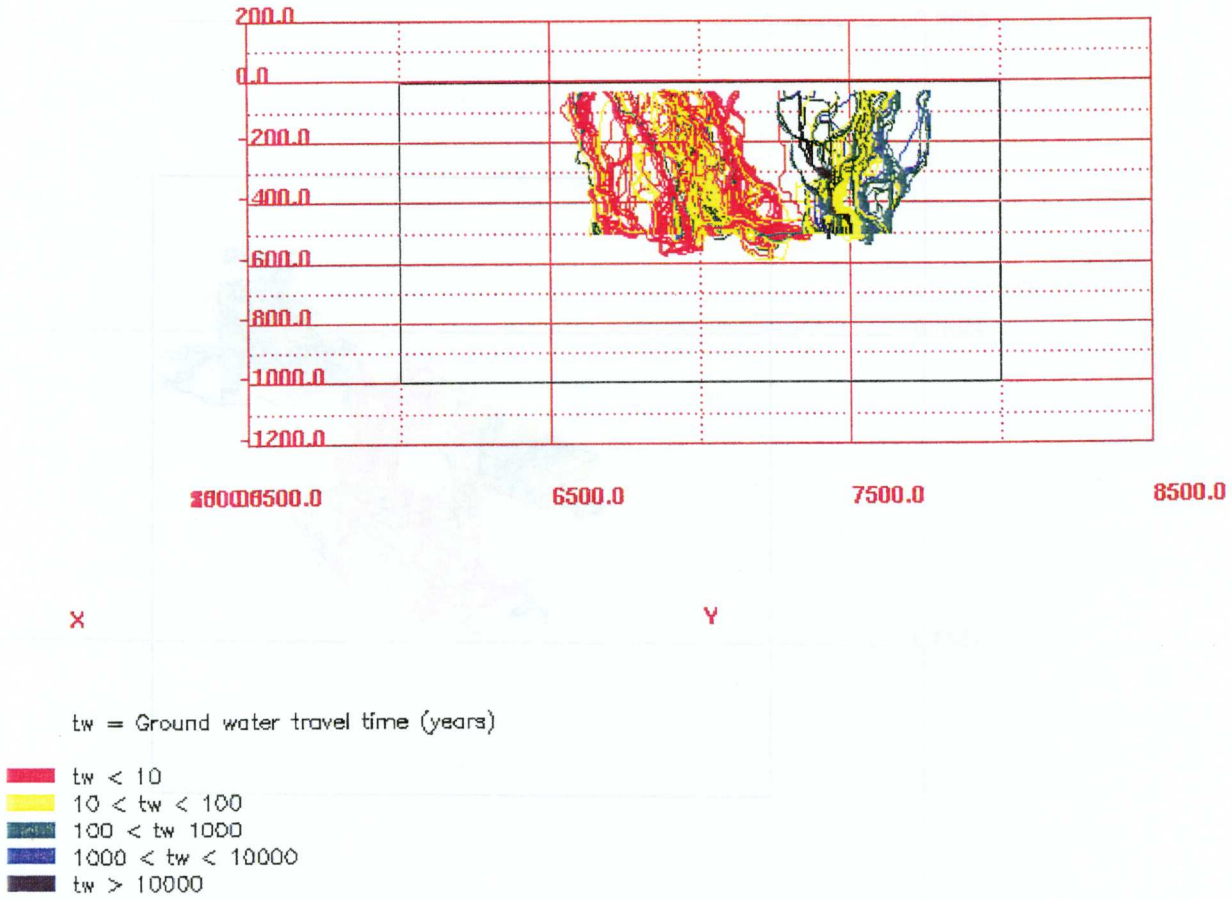

Figure 5-2. *Stream tubes for realisation number 5, elevation view (facing west). The y-positive axis points in the upward direction.*

Table 5-1. Statistical Summary over all canister locations for two realisations (statistics defined in Appendix A).

	Realisation Number	
Log_{10} Travel Time (years) for times < 10000 years	**5**	**13**
Mean	1.517	1.377
Median	1.508	1.445
Variance	0.715	0.563
t_5	0.071	-0.007
t_{25}	0.993	0.899
t_{75}	2.041	1.890
t_{95}	2.982	2.535
D_t	2.912	2.542
Log_{10} Canister Flux (m/year)		
Mean	-3.368	-3.115
Median	-3.406	-3.149
Variance	1.186	1.193
q_5	-5.116	-4.793
q_{25}	-4.079	-3.948
q_{75}	-2.674	-2.354
q_{95}	-1.486	-1.239
D_q	3.631	3.554
Log_{10} F-ratio (yr/m) for times < 10000 years		
Mean	5.607	5.466
Median	5.598	5.535
Variance	0.715	0.563
F_5	4.160	4.083
F_{25}	5.083	4.989
F_{75}	6.131	5.979
F_{95}	7.072	6.625
D_f	2.912	2.542

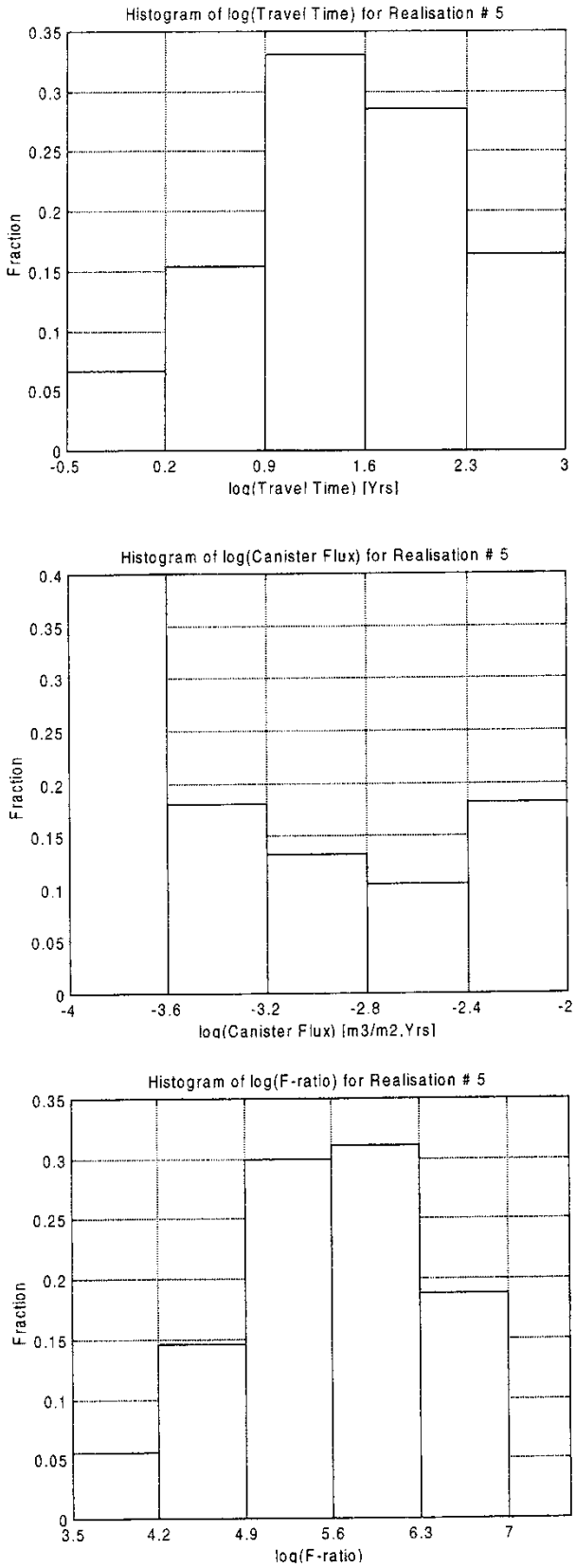

Figure 5-3. *Realisation 5, statistics taken over all canister locations. Histograms of a)log_{10} travel time, b) log_{10} canister flux, and c) log_{10} F-ratio.*

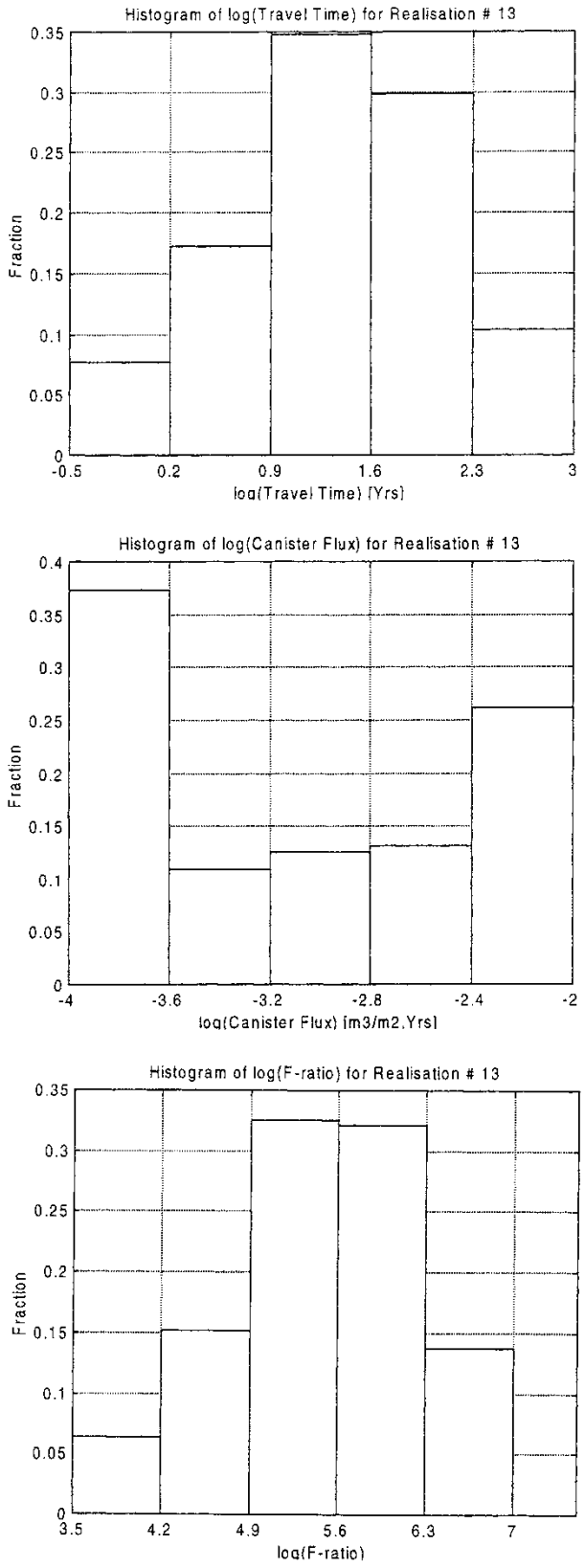

Figure 5-4. *Realisation 13, statistics taken over all canister locations. Histograms of a) log_{10} travel time, b) log_{10} canister flux, and c) log_{10} F-ratio.*

5.2. TYPICAL CANISTERS

Based on preliminary results, this study identifies three typical canister locations based on the following criteria:

- 'typical' transport time/flow in the Western part of the repository
- short transport time/high flow at a NNW-structure in the Eastern part of the repository, and
- rather short transport time from the Southern part of the repository.

Based on these criteria, the selected canister locations are numbers 168, 542 and 885, respectively.

For each of these canister locations, histograms and summary statistics are compiled over all realisations. Table 5-2, and the histograms in Figures 5-5, 5-6, and 5-7 present these results. The median travel times vary widely for these locations, from 1.8 to 35 years. The shortest travel time (at location 542) has the highest canister flux, and the longest travel time (at location 168) has the lowest canister flux. This suggests that $\log_{10}$ travel time is inversely correlated to $\log_{10}$ canister flux.

Table 5-2. Statistical Summary over all Realisations for three canister locations (statistics defined in Appendix A).

	Canister Location Number		
Log_{10} Travel Time (years) for times < 10000 years	**168**	**542**	**885**
Mean	1.511	0.361	0.687
Median	1.545	0.248	0.705
Variance	0.250	0.298	0.533
t_5	0.411	-0.530	-0.562
t_{25}	1.138	0.011	0.152
t_{75}	1.829	0.666	1.046
t_{95}	2.189	1.328	1.940
D_t	1.778	1.858	2.503
Log_{10} Canister Flux (m/year)			
Mean	-3.189	-1.802	-2.356
Median	-3.120	-1.617	-2.407
Variance	0.701	0.662	0.923
q_5	-4.853	-3.812	-4.702
q_{25}	-3.627	-2.223	-2.824
q_{75}	-2.895	-1.374	-1.726
q_{95}	-1.819	-0.892	-1.198
D_q	3.034	2.920	3.505
Log_{10} F-ratio (year/m) for times < 10000 years			
Mean	5.601	4.451	4.777
Median	5.635	4.338	4.795
Variance	0.250	0.298	0.533
F_5	4.501	3.560	3.527
F_{25}	5.228	4.100	4.242
F_{75}	5.918	4.756	5.136
F_{95}	6.279	5.418	6.030
D_f	1.778	1.858	2.503

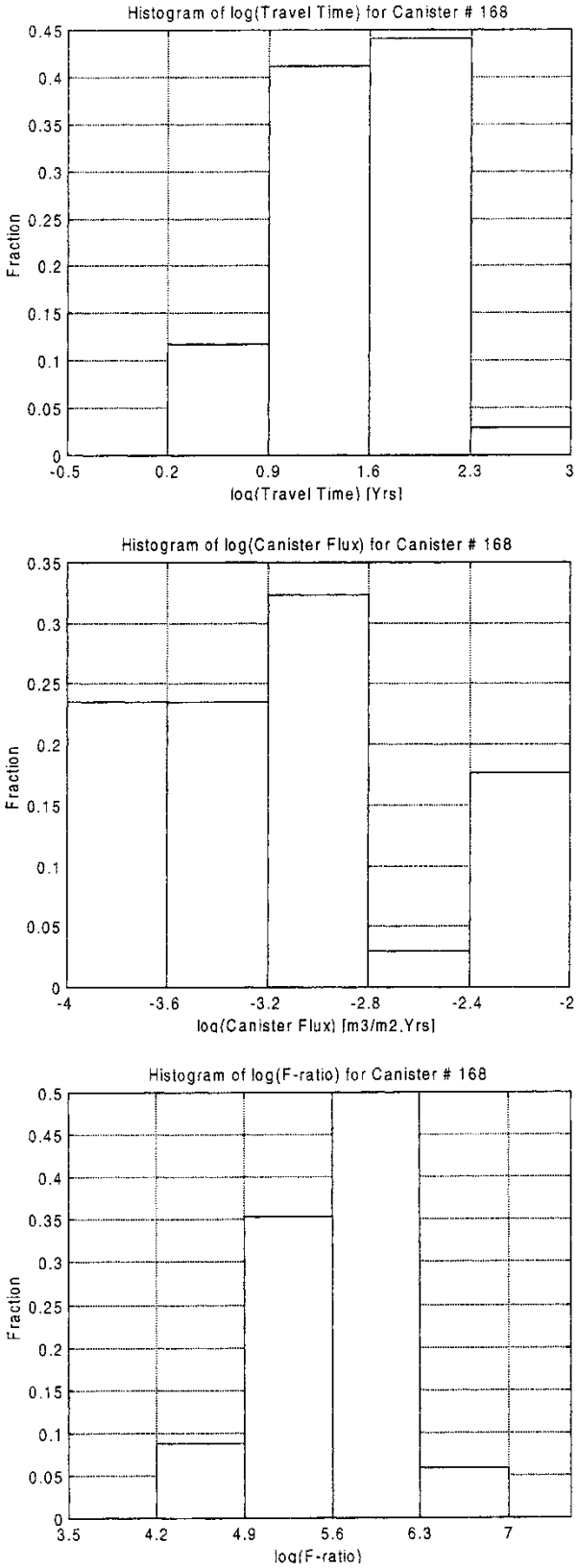

Figure 5-5. *Canister number 168, statistics taken over all realisations. Histograms of a) log_{10} travel time, b) log_{10} canister flux, and c) log_{10} F-ratio.*

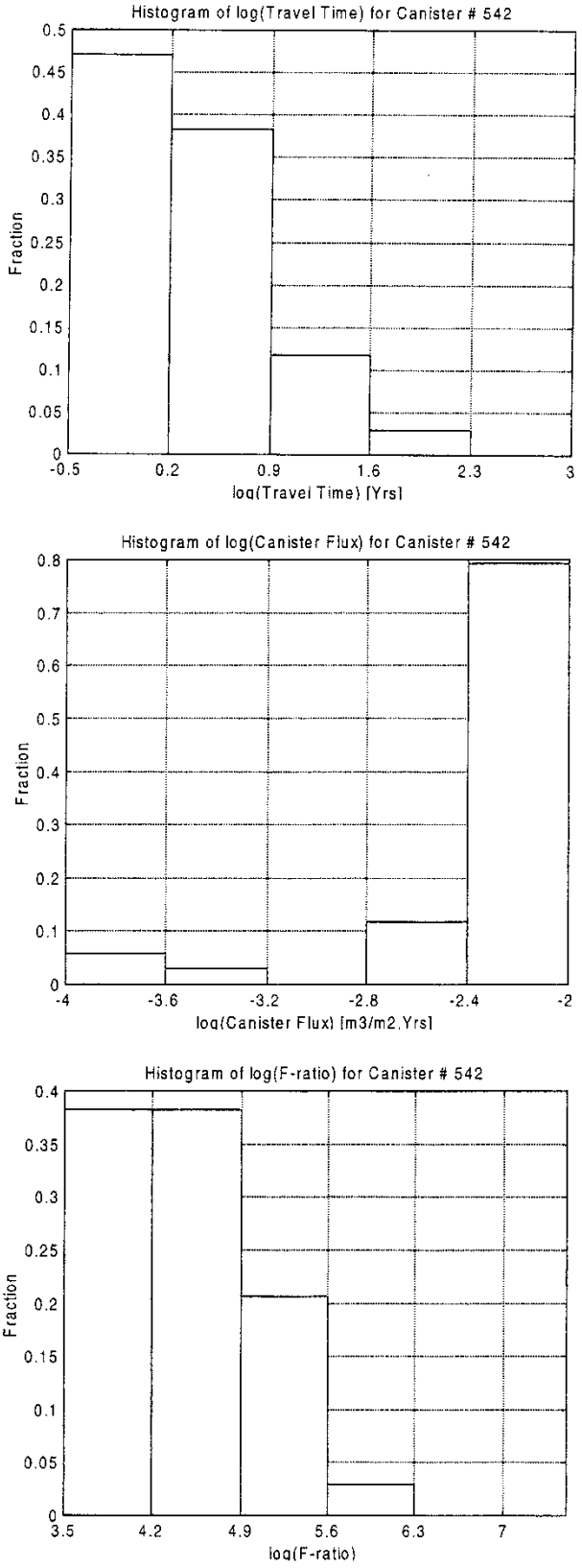

Figure 5-6. *Canister number 542, statistics taken over all realisations. Histograms of a) log_{10} travel time, b) log_{10} canister flux, and c) log_{10} F-ratio.*

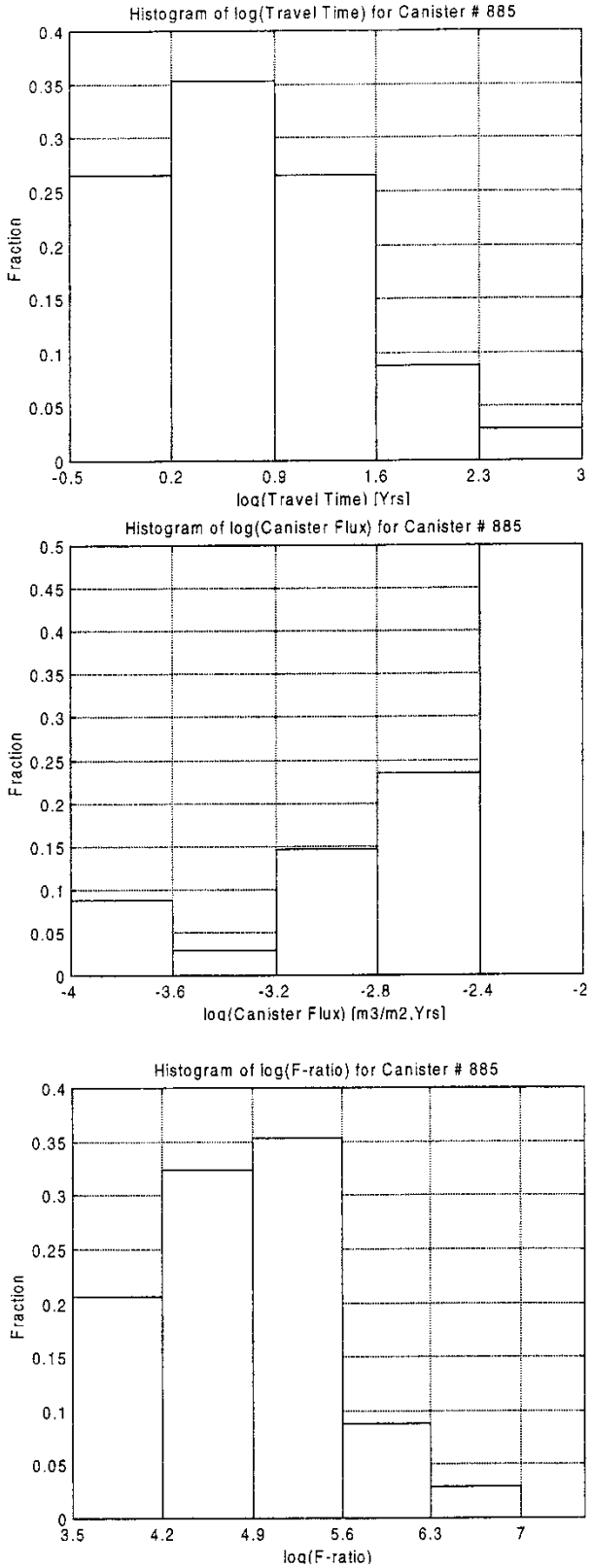

Figure 5-7. *Canister number 885, statistics taken over all realisations. Histograms of a) log_{10} travel time, b) log_{10} canister flux, and c) log_{10} F-ratio.*

5.3. VARIABILITY BETWEEN REALISATIONS

In addition to examining the variability of individual realisations and canister locations, this study also examines the variability between realisations of the ensemble. This is done by computing summary statistics for each realisation alone, then examining the behaviour of these statistics over the set of realisations (i.e., the statistics are computed for each realisation, then summarised over the ensemble). As was discussed in Section 4.1, the number of realisations is somewhat limited, which may limit the reliability of the higher-order moments.

The results comparing the variability between realisations are presented in Table 5-3 and Figures 5-8, 5-9 and 5-10. The variance of the mean suggests that the mean travel time of a realisation changes very little from one realisation to the next. As discussed previously, the F-ratio is a multiple of travel time in HYDRASTAR, resulting in nearly identical behaviour of travel time and F-ratio. The statistics also indicate that the canister fluxes are somewhat more variable than the other performance measures.

Unfortunately, the number of realisations is relatively low (34 realisations), which makes it difficult to infer the distribution and stability of these statistics. For example, if the mean of a realisation is an independent random variable, identically distributed for every realisation, then it might have a normal distribution (e.g., 5-8a, 5-9a, and 5-10a). Similarly, the variance might have a chi-squared distribution (e.g., 5-8c, 5-9c, and 5-10c). Looking at the plots, it is difficult to conclude that this is true or false.

Table 5-3. Realisation statistics, summarised over all realisations (statistics defined in Appendix A).

	Log_{10}Travel Time (years) for times < 10000 years	**Log_{10}Canister Flux (m/yr)**	**Log_{10} F-ratio (yr/m) for times < 10000 years**
Mean of Means	1.405	-3.190	5.495
Median of Means	1.404	-3.172	5.494
Variance of Means	0.019	0.022	0.019
Mean of Variances	0.671	1.096	0.671
Variance of Variances	0.016	0.025	0.016
Median of Medians	1.442	-3.195	5.532
U_y	0.578	0.594	0.578
Median of D_y	2.766	3.522	2.766
UD_y	0.980	0.960	0.980

Number of Realisations	34
Number of Canisters	945
Fraction Travel Time < 10000 years	0.940

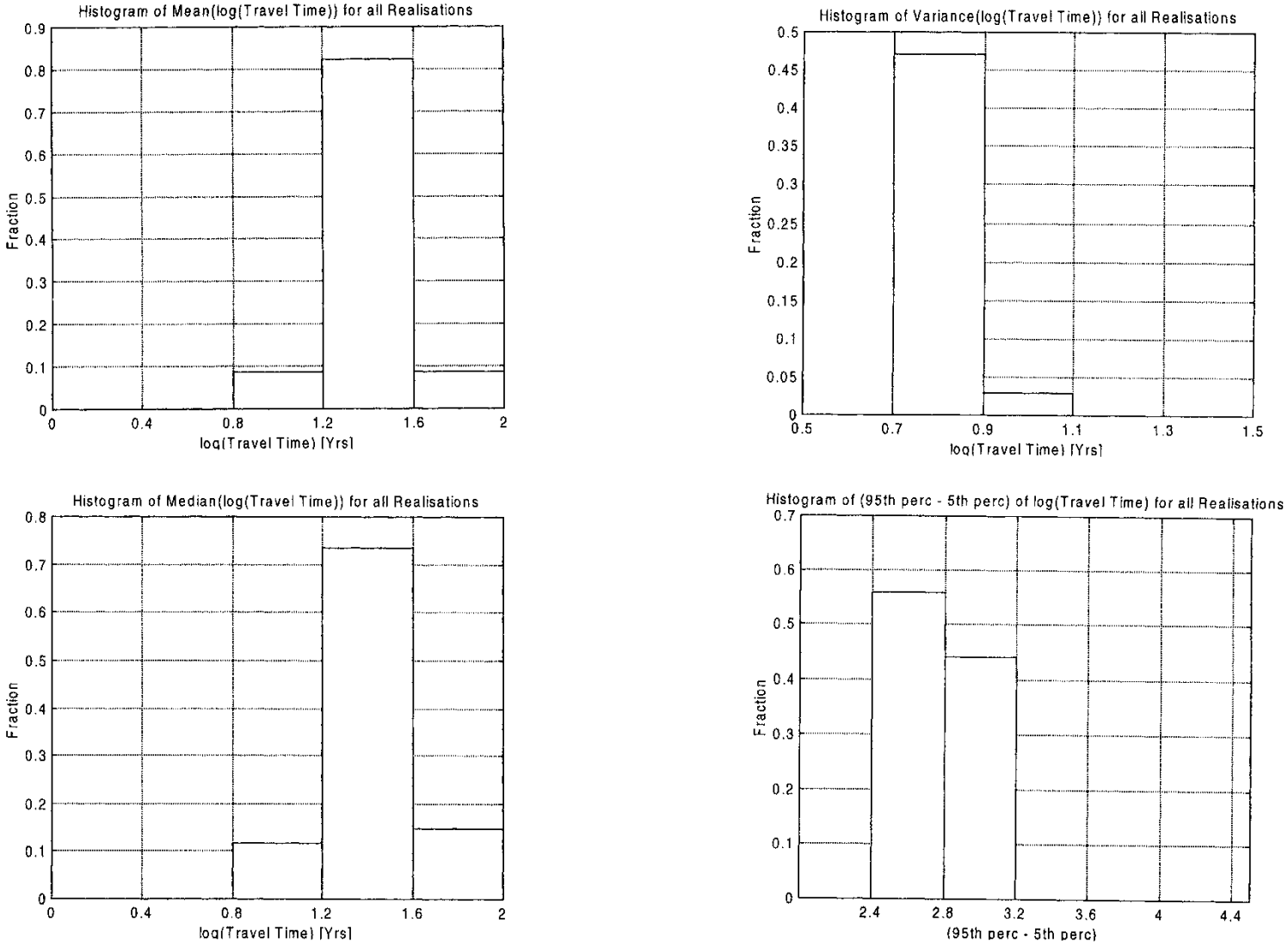

Figure 5-8. *Realisation statistics of log_{10} travel times, summarised over all 34 realisations. Histogram of a) mean, b) median, c) variance, d) D_y.*

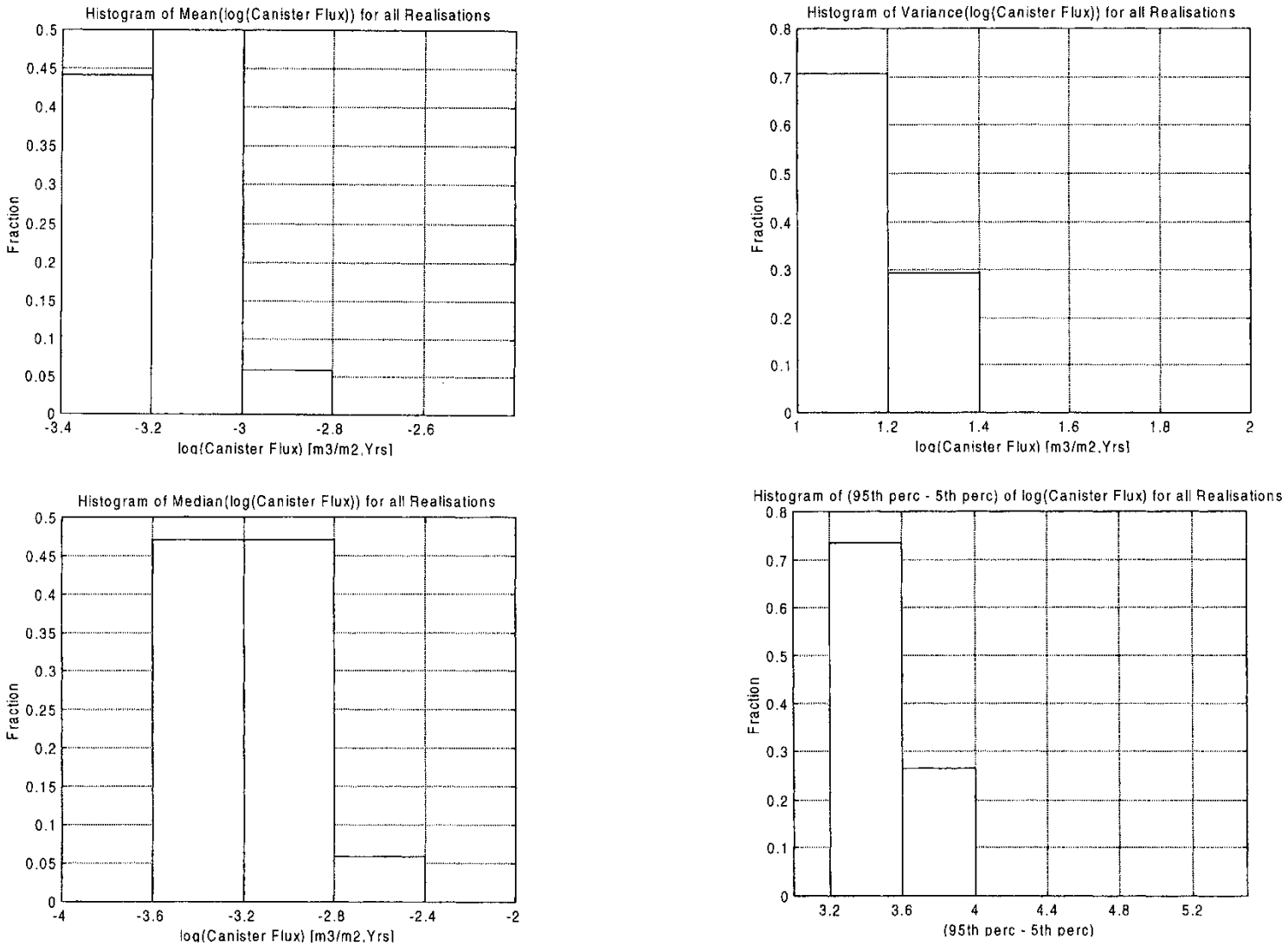

Figure 5-9. *Realisation statistics of log_{10} canister flux, summarised over all 34 realisations. Histogram of a) mean, b) median, c) variance, d) D_y.*

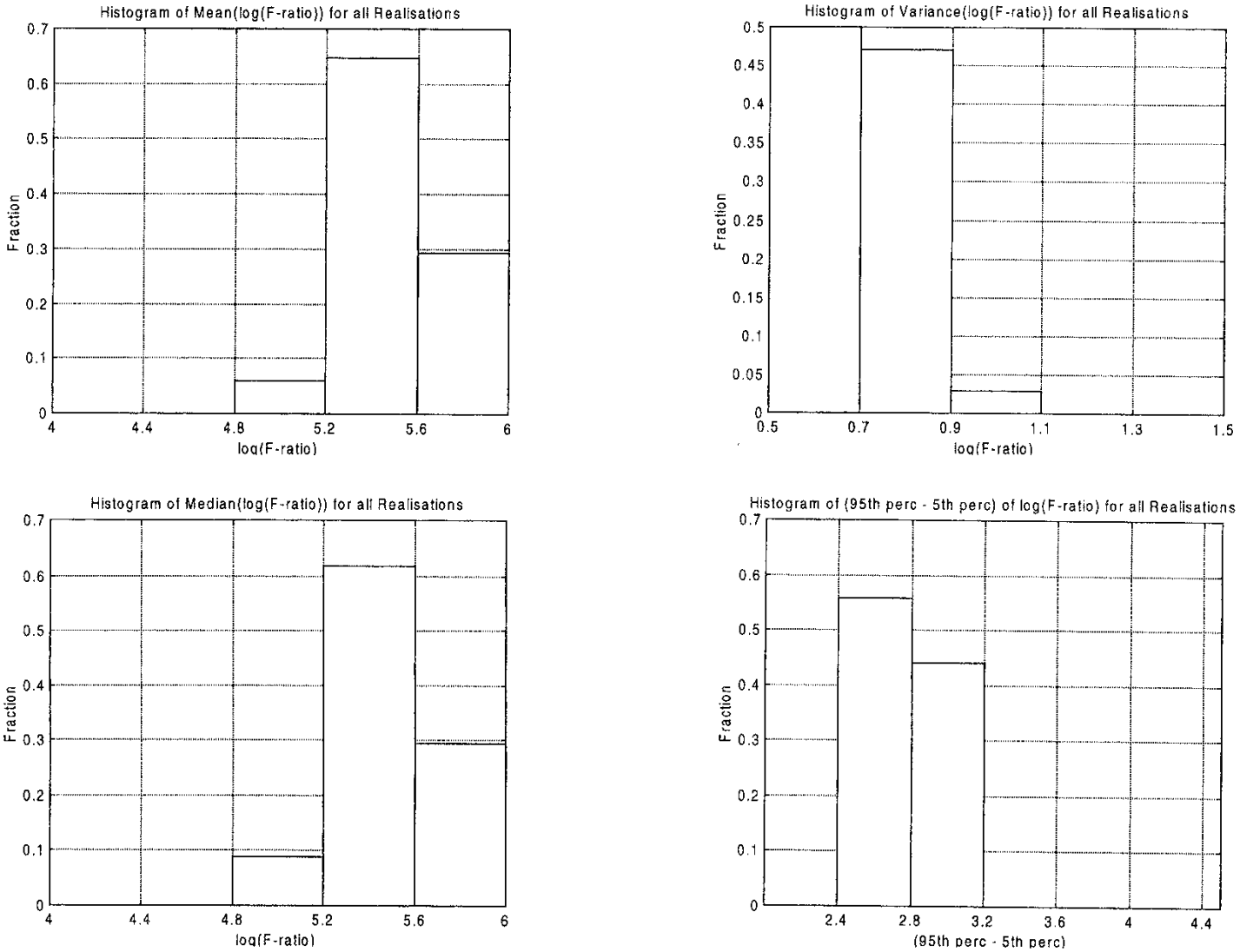

Figure 5-10. *Realisation statistics of log_{10} F-ratio, summarised over all 34 realisations. Histogram of a) mean, b) median, c) variance, d) Dy.*

5.4. ENSEMBLE RESULTS

Table 5-4 summarises the ensemble results, presenting the statistics averaged over all 945 canister locations and all 34 Monte Carlo realisations for travel time, canister fluxes and F-ratios. These ensemble results suggest a median travel time of 27 years, a median F-ratio of 3.3 x 10^5 yr/m. (both with travel paths greater than 10 000 deleted),and a median canister flux of 7.1 x 10^{-4} m/yr.

Table 5-4. Summary statistics for 34 Monte Carlo realisations of 945 canister locations (statistics defined in Appendix A).

	All values			Travel Times > 10,000 years deleted		
	$Log_{10}TT$	$Log_{10}CF$	Log_{10} F-ratio	$Log_{10}TT$	$Log_{10}CF$	Log_{10} F-ratio
Mean	1.563	-3.190	5.653	1.407	-3.155	5.497
Median	1.488	-3.180	5.578	1.429	-3.146	5.519
Variance	1.027	1.116	1.027	0.690	1.099	0.690
5th_perc	0.013	-4.959	4.103	-0.013	-4.916	4.077
25th_perc	0.905	-3.888	4.995	0.863	-3.854	4.953
75th_perc	2.095	-2.479	6.185	1.969	-2.448	6.059
95th_perc	4.000	-1.456	8.090	2.766	-1.427	6.856

5.4.1. Travel Time and F-ratio

In each realisation, HYDRASTAR calculates the travel time for a particle to be advected from each canister location to the model surface. Figure 5-11a presents the frequency histogram for the common logarithm of travel time for 34 realisations, each with 945 starting locations. A series of outliers are seen at the extreme upper tail of the histogram, corresponding to travel times of 10,000 years. These are stream tubes that are intercepted by the side boundaries of the model, and fail to exit the upper surface of the model (Figure 5-1). In this circumstance, HYDRASTAR sets the travel times for these stream tubes to the maximum travel time of 10,000 years. If these stream tubes (approximately 6% of the total number) are deleted from the set, the histogram is as appears in Figure 5-11b. Subsequent experimentation with the boundary locations revealed that if the eastern boundary of the model were shifted farther east, all of the stream tubes would reach the surface of the model. This indicates that the model boundaries as specified by Ström and Selroos (1997) may have been too restrictive.

Table 5-4 presents statistics for travel time and F-ratio for comparison calculated with and without the stream tubes which do not reach the upper surface. The remainder of the analysis includes only the results with travel times less than 10,000 years. Note, however, that this might have unanticipated effects on the dosage calculations.

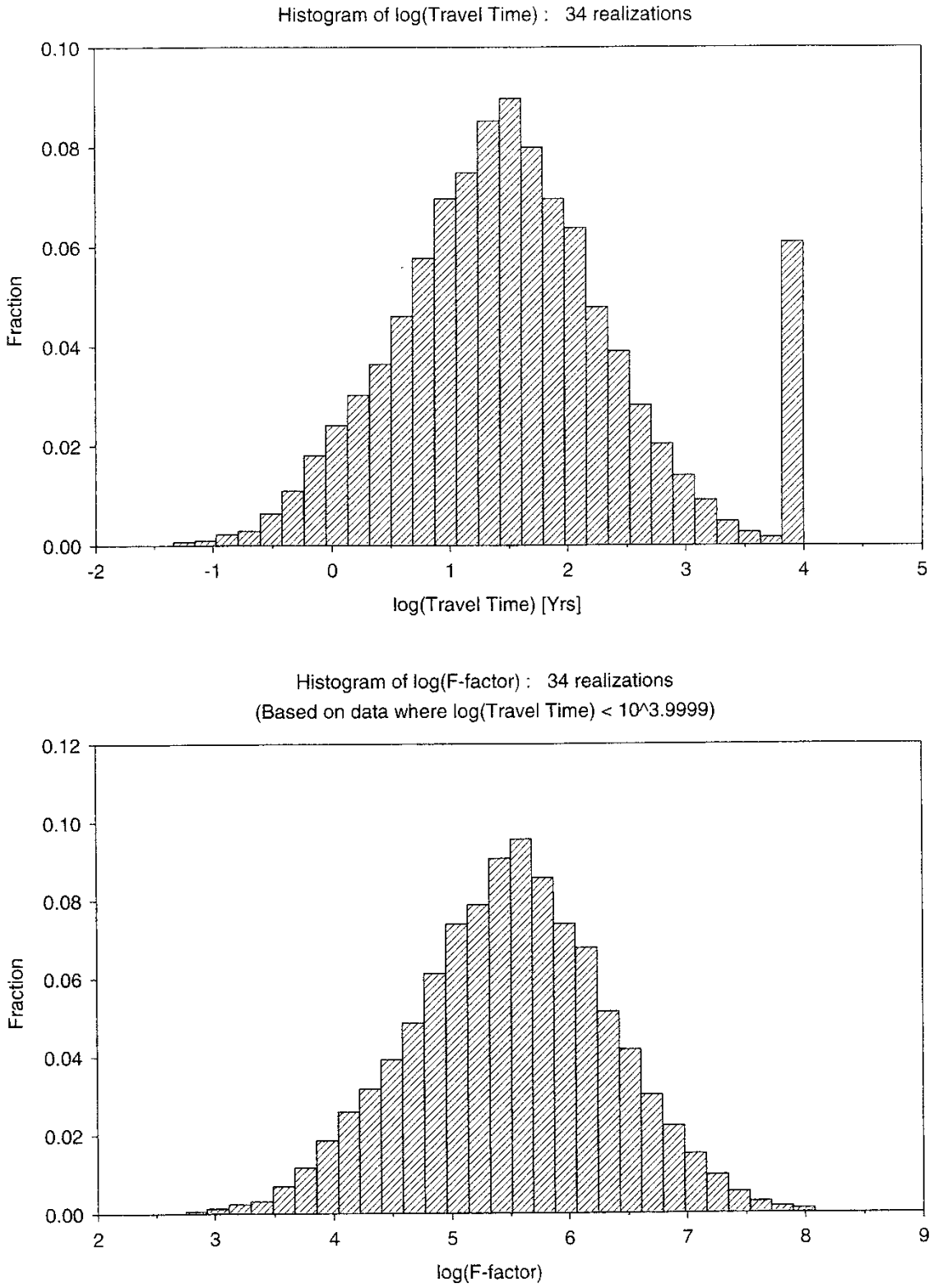

Figure 5-11. *Relative frequency histogram for 34 realisations, each with 945 starting locations for a) $\log_{10}$ travel time and b) $\log_{10}$ travel time with travel times greater than 10,000 omitted.*

Figure 5-12 presents a plot of canister location number (stream tube number) versus the number of realisations with travel time less than 1 year (squares) and less than 10000 years (bars). Stream tubes numbered 820 to 945, which lie in SRD4, have relatively short travel times. Comparing the geometric mean hydraulic conductivities in Table 3-2, note that the hydraulic conductivity of SRD4 is higher than that of SRD3 by more than an order of magnitude (Table 3.2). Stream tubes numbered 450 to 580 also show relatively short travel times. These stream tubes correspond to canister locations that lie in SRD3, in the centre of the hypothetical repository, where deterministic fracture zones NNW-1, NNW-4, and NNW-7 cut through the repository. The stream tubes starting from these canister locations consequently reflect the increased hydraulic conductivity of these fracture zones.

It is important to note that HYDRASTAR allows only a homogenous flow porosity to be specified for the entire domain. This means that, although the advective groundwater velocity may vary along a stream tube, the travel time in any stream tube is directly proportional to this homogeneous flow porosity. This study simply uses the flow porosity provided in the memo by Ström and Selroos (1997) of $\varepsilon_f = 1 \times 10^{-4}$ without further analysis.

In a previous study, Svensson (1997b, cited in Rhén et al., 1997) used the PHOENICS groundwater flow and transport model to determine advective travel times from -450masl to ground surface. Using an average flow porosity of $\varepsilon_f = 4 \times 10^{-3}$, Svensson found that 15% of advective particles would have reached the surface after 100 years. Although Svensson's model used a spatially variable flow porosity, the results can be roughly rescaled to a flow porosity of $\varepsilon_f = 1 \times 10^{-4}$ by dividing the travel times by 10 (i.e., 15% of the streamtubes would have arrived at ground surface after 10 years). This suggests that the travel times of this study are comparable to those of Svensson (1997b).

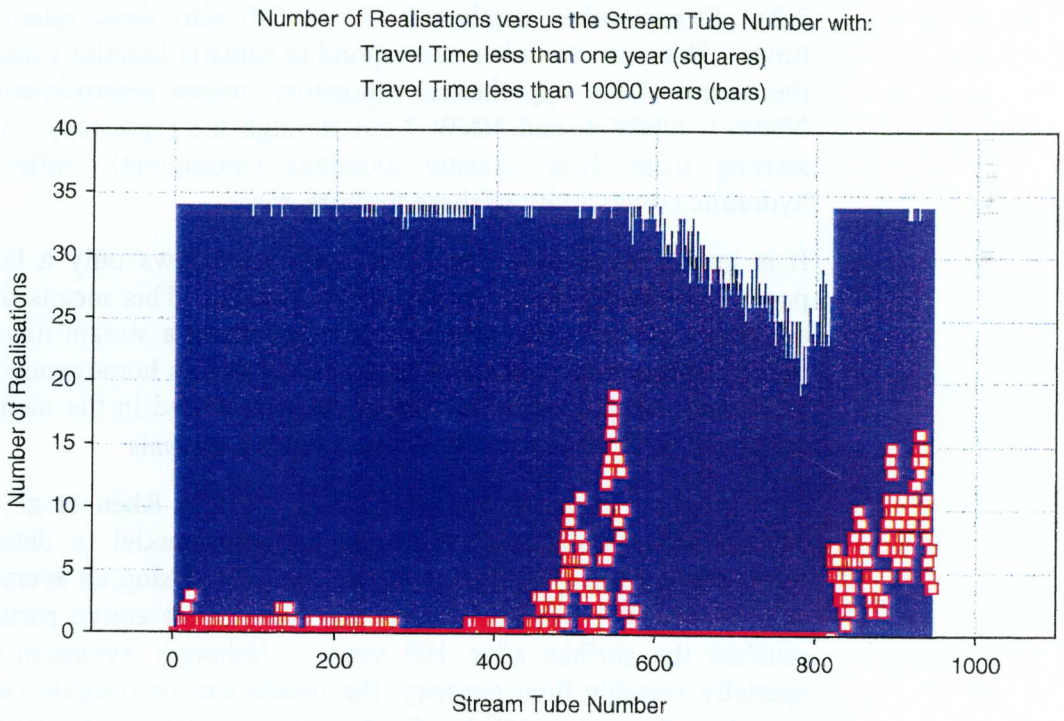

Figure 5-12. *Number of realisations with travel times less than 1 year (boxes) and less than 10000 years (bars), by stream tube number (starting location).*

5.4.2. Canister flux

HYDRASTAR calculated the canister fluxes (Darcy groundwater velocity) at each of the 945 canister locations. Table 5-4 summarises the results for the canister flux, which indicate a median canister flux of 7.1 x 10^{-4} m/year. Figure 5-13 presents the frequency histogram for the common logarithm of canister flux for 34 realisations, each with 945 starting locations. As with the histogram of log travel time, this histogram is also symmetric. Figure 5-14 indicates the logarithm of travel time is inversely correlated to the logarithm of canister flux. This might not be true for models that use a spatially variable porosity or for those with weaker spatial correlation of $\log_{10}$ hydraulic conductivity.

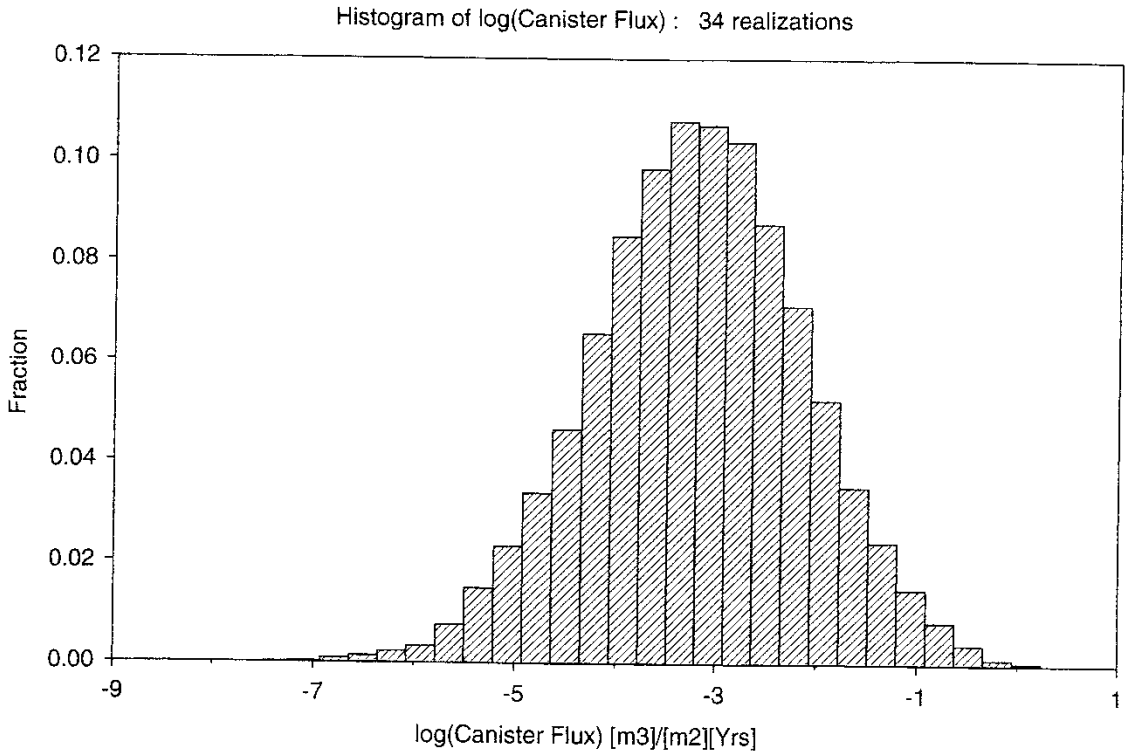

Figure 5-13. *Log_{10} canister flux for 34 realisations, each with 945 starting locations.*

5.4.3. Exit Locations

HYDRASTAR calculated the exit locations for each of the stream tubes. Figure 5-15 presents a map of the exit locations on the model surface (-50 masl). As discussed in Section 5.1, the flow paths are predominantly upward, reflecting the pattern of regional upward groundwater flow. The stream tubes are also directed southward to release locations in the shallow waterways just south of Äspö Island, reflecting the pattern of precipitation recharge on the island, deflecting the stream tubes as groundwater discharges to the surrounding Baltic Sea. A similar effect is observed in the northeastern areas of the repository, which are influenced by the recharge under Mjälen. Note also that several stream tubes reach the side boundary of the model in this area and fail to exit the upper surface of the model. This suggests that the model domain should be extended slightly to the east.

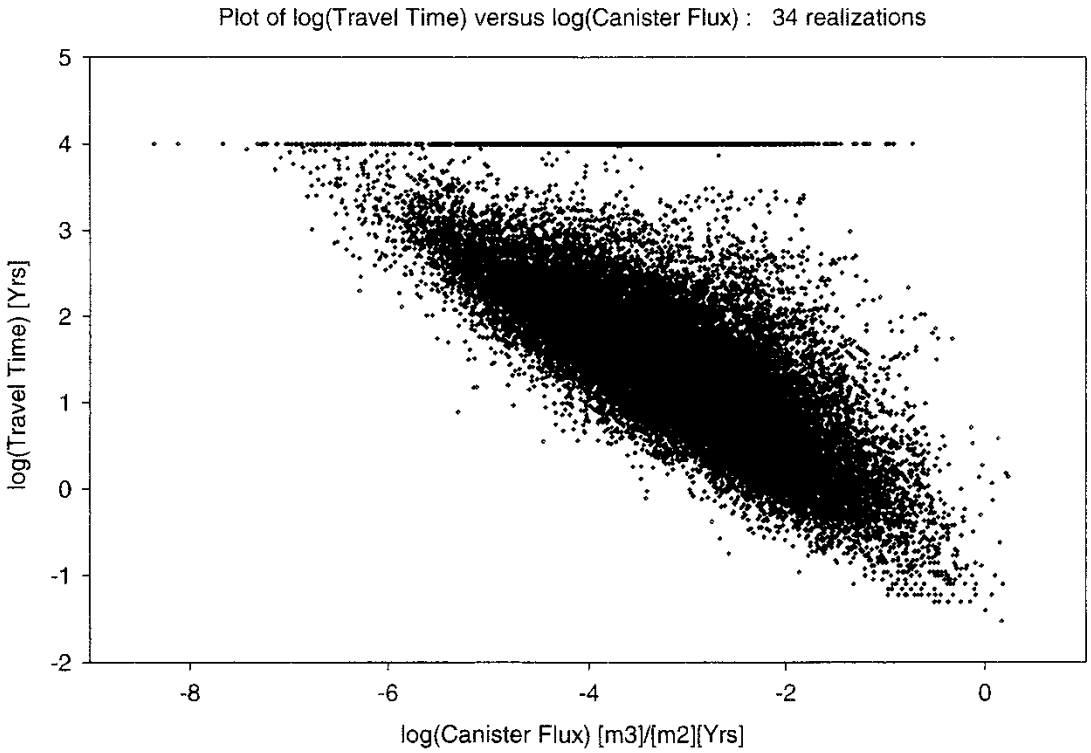

Figure 5-14. *Log_{10} travel time versus log_{10} canister flux for 34 realisations, each with 945 starting locations.*

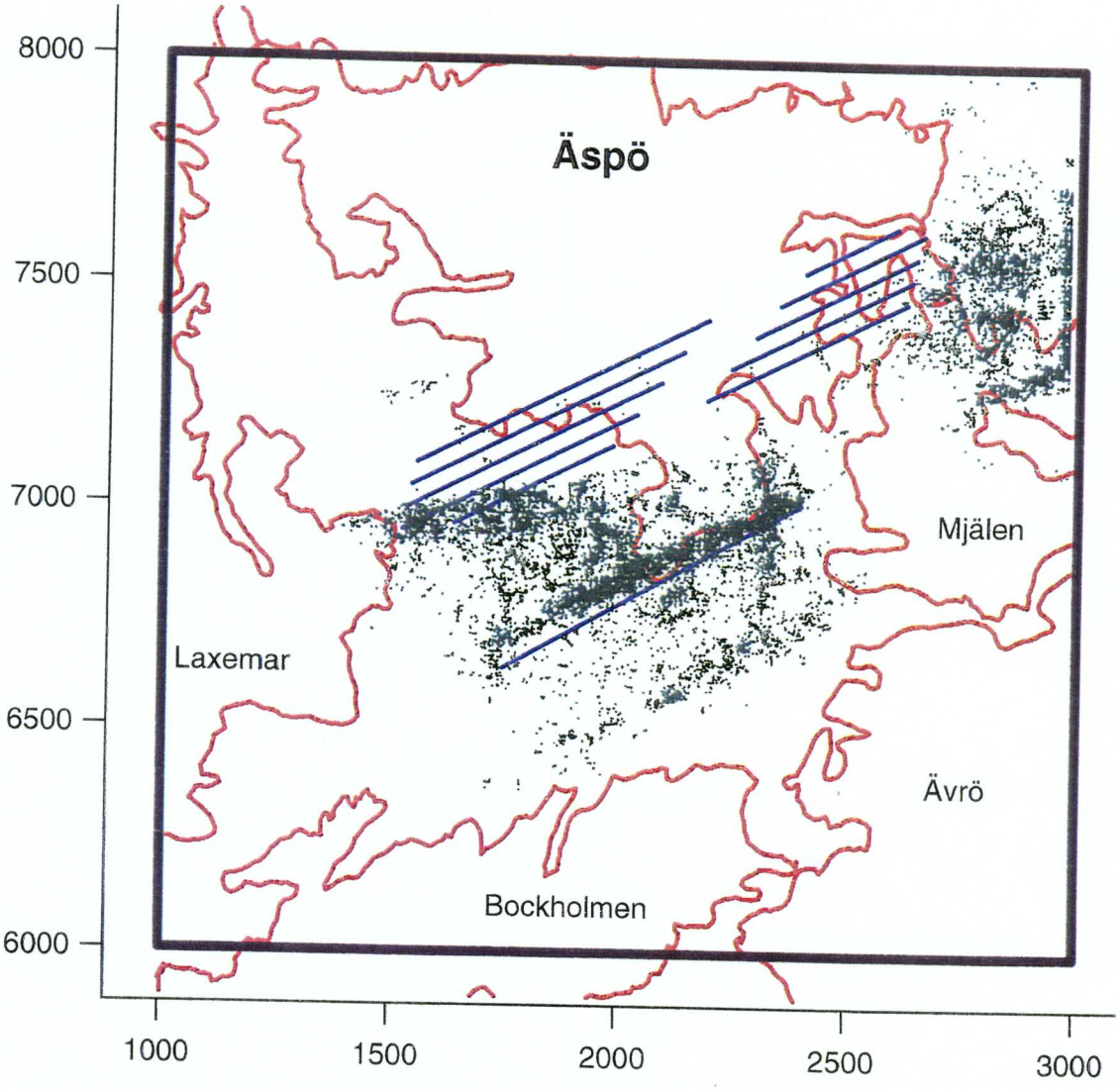

Figure 5-15. *Exit locations for 34 realisations, each with 945 starting locations.*

6. DISCUSSION AND CONCLUSIONS

The Alternative Models Project (AMP) is part of the SKB SR 97 study, and is a comparison of three alternative modelling approaches to bedrock PA at the Aberg site. This study is an application of HYDRASTAR, a stochastic continuum groundwater flow and transport modelling program. The application is relatively straightforward, with the majority of the model parameters and boundary conditions explicitly specified by SKB in the project requirements memo by Ström and Selroos (1997).

6.1. SUMMARY AND DISCUSSION

The parameters are unchanged from those given in Ström and Selroos (1997), except that the hydraulic conductivities are adjusted as suggested by Svensson (1997) and rescaled as suggested by Walker et al. (1997). The SKB geostatistical analysis code INFERENS is used to infer a regularised variogram model, based on the 3m interpreted hydraulic conductivities taken from SICADA. Unconditional geostatistical simulation is then used for multiple realisations of the hydraulic conductivity field.

Ström and Selroos (1997) provide the boundary conditions for this model. These are constant head boundaries, derived from a single stochastic realisation of a regional scale model by Svensson (1997). The overall flow pattern of the regional model is typical of coastal areas: topographically driven flow from the inland areas exiting to the coastal waters. The transfer of regional heads via constant head boundaries preserves this pattern in the site-scale model. The boundary fluxes of the single realisation are also provided to facilitate mass balance calculations. The median boundary flux across the site-scale domain is slightly greater than that of the regional model. However, the single realisation of the regional model might not represent the expected boundary conditions, which limits the applicability of the fine-tuning of rescaling with respect to mass balance proposed by Walker et al. (1997). Adjustment of hydraulic conductivity to fine-tune the rescaling is not pursued.

The study uses 34 realisations of 945 canister locations to evaluate the travel times, canister fluxes, and F-ratios for the proposed repository. Two comparisons are made of the results, one using two realisations of the set of 34, and another using three canister locations from the set of 945. The two realisations are examined to illustrate the variability within individual realisations. The individual realisations are selected as being typical with respect to travel time and canister flux. Because the porosity is uniform in the model, the travel times and canister fluxes are inversely correlated. Consequently, although one realisation is selected based on the travel time and another based on the canister flux, the realisations are quite similar. Three individual canister locations, one from each of the three repository blocks, are examined over all 34 realisations to illustrate differences due to location and the associated uncertainty. The median $\log_{10}$ travel times, F-ratios, and canister fluxes differ dramatically between locations, as do their variances and distributions. Canister positions with relatively high canister flux appear to be

associated with relatively short travel times, suggesting that $\log_{10}$ travel time is inversely correlated to $\log_{10}$ canister flux.

The results of the variability between realisations (i.e., statistics of each realisation, compared among the 34 realisations) are somewhat ambiguous because of the low number of realisations. The variability of the mean, median and variance of $\log_{10}$ travel time, canister flux, and F-ratio appear to be quite low between realisations. The histograms of these statistics were constructed from relatively few realisations, limiting further interpretation.

The ensemble results taken over all canister locations and realisations suggest the following statistics:

- a median travel time of 27 years
- a median canister flux of 7.1×10^{-4} m/yr, and
- a median F-ratio of 3.3×10^{5} yr/m.

As discussed above, the current version of HYDRASTAR is limited to a homogeneous flow porosity over the entire domain. Consequently, the F-ratio is a simple multiple of the travel time, and the canister flux is inversely correlated to the travel time. The $\log_{10}$ travel time and $\log_{10}$ canister flux distributions are symmetric. The flow paths and exit locations of the realisations are compatible with the overall pattern of flow at the site. The explicitly prescribed domain is seen to be slightly restrictive, with 6% of the stream tubes failing to exit the upper surface of the model.

6.2. POSSIBLE MODEL REFINEMENTS

In several respects, the modelling could be improved within the current features of HYDRASTAR. These include:

- The model domain could be extended eastward, to reduce the number of stream tubes failing to exit the model's upper surface.
- A simple sensitivity analysis could identify critical assumptions for boundary conditions, grid spacing, and hydraulic parameters.
- The effect of directly conditioning the hydraulic conductivity simulations on measured hydraulic conductivities is not examined, and might be informative.
- The SRD hydraulic conductivities could be calibrated to observed head measurements, possibly using HYDRASTAR's pilot point calibration algorithm.

Several improvements could be made with respect to the representation of site conditions which are not possible using the current version of HYDRASTAR. These include:

- Rather than converting to equivalent freshwater heads, include the density effects by modelling the salinity explicitly.
- A nonparametric geostatistical simulation algorithm might allow a more realistic representation of the data.

6.3. SUMMARY OF FINDINGS

The findings of this study can be summarised as follows. With regard to the usage of data and consistency with the regional model:

- Input data for the model is unmodified from that given by Ström and Selroos (1997) except for the rescaling of hydraulic conductivities and the adjustment of the value for SRD4.
- The transfer of regional heads to the site-scale model via constant head boundaries preserves the pattern of topographically driven flow at the site.
- The site-scale model slightly over-predicts the boundary fluxes from the single realisation of the regional flow model, however the use of a single realisation of the regional flow model limits the applicability of the fine-tuning of rescaling with respect to mass balance.

With regard to the variability seen within realisations, a examination is made of the results for two realisations, one chosen based on canister flux and the other based on travel time. However, because travel times and canister fluxes are inversely correlated, the realisations are quite similar.

With regard to the variability between locations, three individual canister locations are examined, one from each of the three repository blocks. The median $\log_{10}$ travel times and F-ratios were quite similar, but the median $\log_{10}$ canister fluxes differed.

The variability between realisations is also examined, and shows:

- The variability of the mean, median and variance of $\log_{10}$ travel time, canister flux, and F-ratio appears to be quite low between realisations.
- The histograms of these statistics are inconclusive as a result of too few realisations.

The ensemble results taken over all realisations and all canister locations suggest:

- A median travel time of 27 years.
- A median canister flux of 7.1×10^{-4} m/yr.
- A median F-ratio of 3.3×10^{5} yr/m.
- The canister flux is inversely correlated to the travel time.
- Flow paths and exit locations are compatible with the regional flow pattern.

The modelling could be improved within the current features of HYDRASTAR, including extending the domain, sensitivity analysis and calibration. Other refinements lie outside of the HYDRASTAR abilities.

REFERENCES

Dagan G, 1986. Statistical theory of groundwater flow and transport: pore to laboratory, laboratory to formation, and formation to regional scale. Water resources Research, Vol. 22:9.

de Marsily G, Lavedan C, Boucher M, Fasanino G, 1984. Interpretation of Interference Tests in a Well Field Using Geostatistical Techniques to Fit the Permeability Distribution in a Reservoir Model, in Geostatistics for Natural Resources Characterization. Second NATO Advanced Study Institute, GEOSTAT 1983, Tahoe City, California. Edited by G Verly, M David, A G Journel, and A Marachal, pp. 831-849, D Reidel, Hingham, Mass,USA.

Eriksson L O, Oppelstrup J, 1994. Calibration with respect to hydraulic head measurements in stochastic simulation of groundwater flow - A numerical experiment using MATLAB. SKB Technical Report TR 94-30 Stockholm, Sweden.

Geier J, 1993a. Verification of the geostatistical inference code INFERENS, Version 1.1, and demonstration using data from Finnsjön. SKB Technical Report TR 93-09, Stockholm, Sweden.

Geier J, 1993b. Version 1.0 User's Guide to INFERENS 1.1. SKB AR 93-24.

Hammersley, JM and Handscomb, DC, 1975. Monte Carlo Methods, Methuen, London.

Hodgkinson D P, Barker J, 1985. Specification of a Test Problem for HYDROCOIN Level 1 Case1: Transient Flow from a Borehole in a Fractured Permeable Medium, Report AERE R-11574, UK Atomic Energy Authority, Harwell Laboratories, UK.

Journel A G, Huijbregts Ch J, 1978. Mining Geostatistics, Academic Press.

La Pointe P R, 1994. Evaluation of stationary and non-stationary geostatistical models for inferring hydraulic conductivity values at Äspö. SKB Technical Report TR 94-22.

Larsen, RJ, and Marx, ML, 1986. An Introduction to Mathematical Statistics and its Applications, Prentice-Hall, London.

Lovius L, Eriksson L, 1993. Verification of HYDRASTAR version 1.4. SKB Working report AR 93-46, Stockholm, Sweden.

Lovius L, Eriksson L, 1994. Development of a Transient Version of HYDRASTAR. SKB Working report AR 94-12, Stockholm, Sweden.

Morris S T, Cliffe K A, 1994. Verification of HYDRASTAR: Analysis of hydraulic conductivity fields and dispersion. SKB Technical Report TR 94-21, Stockholm, Sweden.

Munier, R, Sandstedt, H, Niland L, 1997. Förslag till principiella utformningar av förvar enligt KBS-3 för Aberg, Beberg and Ceberg. SKB R 97-09.

Niemi A, 1995. Modelling of Äspö hydraulic conductivity data at different scales by means of 3-dimensional Monte Carlo simulations. SKB ICR 95-08.

Norman S, 1991. Verification of HYDRASTAR - A code for stochastic continuum simulation of groundwater flow. SKB Technical Report TR 91-27, Stockholm, Sweden.

Norman S, 1992a. Statistical inference and comparison of stochastic models for the hydraulic conductivity at the Finnsjön-site. SKB Technical Report TR 92-08, Stockholm, Sweden.

Norman S, 1992b. HYDRASTAR - A code for stochastic simulation of groundwater flow. SKB Technical Report TR 92-12, Stockholm Sweden.

OECD, 1983. The International HYDROCOIN Project: Groundwater hydrology modelling strategies for performance assessment of nuclear waste disposal. Level: Code verification.

Rhén I, Gustafson G, Stanfors R, Wikberg P. 1997. Äspö Hard Rock Laboratory – Geoscientific Evaluation 1997/5. Models based on site characterisation 1986-1995. SKB TR 97-06.

Rubin Y, Gómez-Hernández J J, 1990. S stochastic Approach to the problem of Upscaling of conductivity in disordered media: Theory and unconditional numerical simulations. Water Resources Research, Vol. 26:4.

SKB, 1992. SKB 91: Final disposal of spent nuclear fuel. Importance of bedrock for safety. SKB Technical Report TR 92-20, Stockholm, Sweden.

SKB, 1996a. Template for safety reports with descriptive example, SKB TR 96-05.

SKB, 1996b. User's Guide to HYDRASTAR 1.5. SKB Progress Report PR U-96-15.

Ström A., Selroos J-O., 1997. SR 97 – Use of alternative models for describing flow and transport in the far field, SKB PM 1997 – 4 – 25.

Svensson U, 1997. A regional analysis of groundwater flow and salinity distribution in the Äspö area. SKB Technical Report TR 97-09, Stockholm, Sweden.

Svensson U, 1997b. A site scale analysis of groundwater flow and salinity distribution in the Äspö area. SKB Technical Report TR 97-17, Stockholm, Sweden.

Walker D, and Bergman, B, 1997. Verification of HYDRASTAR v.1.5 Inverse Modelling, SKB Progress Report, in preparation.

Walker D, Lovius L, Eriksson L, 1997. Verification of HYDRASTAR 1.7: Nugget effect in geostatistical simulations, SKB Progress Report U-97-22.

Walker D., Rhén I., Gurban I., 1997. Summary of Hydrogeologic Conditions at Aberg, Beberg and Ceberg. SKB Technical Report TR 97-23, Stockholm, Sweden.

Ward D, Buss D, Mercer J, Hughes S, 1987. Evaluation of a groundwater corrective action at the Chem-Dyne hazardous waste site using a telescopic mesh refinement modeling approach, Water Resour. Res., 23(4), pp. 603-617.

Wikberg P, Gustafson G, Rhén I, Stanfors R. 1991. Äspö Hard Rock Laboratory. Evaluation and conceptual modelling based on the pre-investigations 1986-1990. SKB TR 91-22.

Winberg, A, 1994. Geostatistical analysis of transmissvity data from fracture zones at Äspö, SKB Progress Report PR 25-94-17.

APPENDIX A. DEFINITION OF STATISTICAL MEASURES

Define an entity of interest such as canister flux (q), travel time (t) and F-ratio (F), and their respective $\log_{10}$ transforms as:

$$Y=log_{10}(x) \qquad x=q,\ t\ \ F$$

Then for assessing the results, use the following measures:

histogram of Y

ensemble mean $= \langle Y \rangle$

realisation mean = $\bar{Y}$

ensemble variance = var$[Y]$

realisation variance = σ^2_Y

realisation median $= Y_{50}$

realisation $D_Y = Y_{95} - Y_5$

Ensemble mean of means = $\langle \bar{Y} \rangle$

Ensemble variance of means = var $[\bar{Y}]$

Ensemble mean of variances = $\langle \sigma^2_Y \rangle$

Ensemble variance of variances = var $[\sigma^2_Y]$

Ensemble median of medians = $M_Y = (Y_{50})_{50\%}$

D_Y of medians = $U_Y = (Y_{50})_{95\%} - (Y_{50})_{5\%}$

Median of D_Y = $MD_Y = (D_Y)_{50\%}$

D_Y of D_Y = $UD_Y = (D_Y)_{95\%} - (D_Y)_{5\%}$

APPENDIX B. PARAMETER SOURCES

Mechanisms and model parameters considered in this study when modelling groundwater flow using HYDRASTAR.

Mechanism	HYDRASTAR model parameter Symbol (unit)	Description	Source
Topographically driven flow	-	Fracture zone and rock domain geometries	Based on the interpreted geologic structural model for the site, TR 97-06.
	T (m^2/s)	Fracture zone transmissivities	Based on the interpreted geohydrological model for the site, TR 97-06, which constitutes a hydraulic synthesis of the available information from fracture zones. Interference tests on 50 to 100m scale as provided in AMP memo, rescaled as described in as described in TR 97-06
	K (m/s)	Rock mass hydraulic conductivity	Based on the interpreted geohydrological model for the site TR 97-06, which constitutes a hydraulic synthesis of the available information for the rock mass. Single-hole water injection tests on 3m scale also used directly for conditional simulation in HYDRASTAR. These data are also the basis for the geostatistical analysis performed with INFERENS. Upscaling as described in TR 97-06
	S_s (m^{-1})	Specific storativity. Necessary for transient simulations.	Not used
	-	Top boundary condition	Constant head, as provided in AMP project memo, from Svensson, 1997.
	-	Vertical/lower boundary conditions	Constant head, as provided in AMP project memo, from Svensson, 1997.
	ε_f (-)	Flow porosity	Needed when calculating travel times for particle tracking, assumed uniform as stipulated in AMP project memo The flow porosity ε_f is poorly known in general .
Thermally and/or salinity driven flow	ρ (kg/m^3)	Groundwater density	Constant density used in AMP.

APPENDIX C. SICADA LOGS FOR ÄSPÖ SITE DATA

C.1 For coordinates and previous interpreted K values

Date: 970324 18:02:21

Table(s): transient_inj_cd

Columns :transient_inj_cd.idcode, transient_inj_cd.start_date, transient_inj_cd.stop_date, transient_inj_cd.seclen, transient_inj_cd.secup, transient_inj_cd.bc, transient_inj_cd.k_steady_state, transient_inj_cd.k_injection, transient_inj_cd.k_fall_off, transient_inj_cd.k_jacob, transient_inj_cd.k_prel, transient_inj_cd.k, transient_inj_cd.skinfactor_i, transient_inj_cd.skinfactor_t, transient_inj_cd.spec_cap, transient_inj_cd.goodness, transient_inj_cd.test_date, transient_inj_cd.comment

New Columns: midpoint

Condition: Expr=secup+(seclow-secup)/2

Criteria: (transient_inj_cd.idcode ='KAS02' OR

transient_inj_cd.idcode ='KAS03' OR transient_inj_cd.idcode ='KAS04' OR

transient_inj_cd.idcode ='KAS05' OR transient_inj_cd.idcode ='KAS06' OR

transient_inj_cd.idcode ='KAS07' OR transient_inj_cd.idcode ='KAS08' OR

transient_inj_cd.idcode ='KLX01') AND transient_inj_cd.seclen =3

Result: 1300 rows written

Filename: trans_l.csv

Fileformat: CSV

Coordinate system: Local

Coordinate calculation column: midpoint

C.2 For rock/conductor codes and Rhén K values

Date :970324 18:05:05

Tables :sic_dba.transient_inj_cd

Columns :transient_inj_cd.idcode, transient_inj_cd.start_date, transient_inj_cd.stop_date, transient_inj_cd.seclen, transient_inj_cd.secup, transient_inj_cd.bc, transient_inj_cd.k_steady_state, transient_inj_cd.k_injection, transient_inj_cd.k_fall_off, transient_inj_cd.k_jacob, transient_inj_cd.k_prel, transient_inj_cd.k, transient_inj_cd.skinfactor_i, transient_inj_cd.skinfactor_t, transient_inj_cd.spec_cap, transient_inj_cd.goodness, transient_inj_cd.test_date, transient_inj_cd.comment

New Columns: midpoint

Condition: Expr=secup+(seclow-secup)/2

Criteria: (transient_inj_cd.idcode ='KAS02' OR

transient_inj_cd.idcode ='KAS03' OR transient_inj_cd.idcode ='KAS04' OR

transient_inj_cd.idcode ='KAS05' OR transient_inj_cd.idcode ='KAS06' OR

transient_inj_cd.idcode ='KAS07' OR transient_inj_cd.idcode ='KAS08' OR

transient_inj_cd.idcode ='KLX01') AND transient_inj_cd.seclen =3

Result: 1300 rows written

Filename: trans_r.csv

Fileformat: CSV

Coordinate system: RT

Coordinate calculation column: midpoint

Output to: File

Date :970606 15:31:46

Table(s) :sic_dba.zone_model96

Columns :zone_model96.site, zone_model96.idcode,
zone_model96.borehole, zone_model96.sub_secup,
zone_model96.sub_seclow,
zone_model96.zone_name, zone_model96.rocktype,
zone_model96.k,
zone_model96.k_source, zone_model96.qc_ok,

Criteria :1=1

Result : 1300 rows written to file.

Filename : /home/skbee/rhen_k.csv

File format : csv

APPENDIX D. LOCATION OF DATA FILES

All data files, both input data and raw results are available on the SKB file system under the directory

`/net/s92/export/home/tmp-hyd/amp/ampbas`

A full listing including size and file date is shown below.

```
 1780818 Jun  8 01:24 DX1.distribution
 1780818 Jun  8 01:25 DX2.distribution
 1780818 Jun  8 01:25 DY1.distribution
 1780818 Jun  8 01:25 DY2.distribution
 3607298 Jun  8 01:26 DZ1.distribution
 3607298 Jun  8 01:27 DZ2.distribution
  405 Jun  6 07:23 HYDR11.dt
61425 Jun  6 08:16 ampbas.canister_flux1
61425 Jun  6 16:32 ampbas.canister_flux10
61425 Jun  6 17:46 ampbas.canister_flux11
61425 Jun  6 18:42 ampbas.canister_flux12
61425 Jun  6 21:04 ampbas.canister_flux13
61425 Jun  6 22:19 ampbas.canister_flux14
61425 Jun  6 23:15 ampbas.canister_flux15
61425 Jun  7 00:25 ampbas.canister_flux16
61425 Jun  7 01:41 ampbas.canister_flux17
61425 Jun  7 02:45 ampbas.canister_flux18
61425 Jun  7 04:14 ampbas.canister_flux19
61425 Jun  6 09:03 ampbas.canister_flux2
61425 Jun  7 05:58 ampbas.canister_flux20
61425 Jun  7 07:15 ampbas.canister_flux21
61425 Jun  7 08:19 ampbas.canister_flux22
61425 Jun  7 09:27 ampbas.canister_flux23
61425 Jun  7 10:17 ampbas.canister_flux24
61425 Jun  7 11:33 ampbas.canister_flux25
61425 Jun  7 12:52 ampbas.canister_flux26
61425 Jun  7 14:25 ampbas.canister_flux27
61425 Jun  7 15:40 ampbas.canister_flux28
61425 Jun  7 17:26 ampbas.canister_flux29
61425 Jun  6 09:56 ampbas.canister_flux3
61425 Jun  7 18:46 ampbas.canister_flux30
61425 Jun  7 20:30 ampbas.canister_flux31
```

```
61425 Jun  7 22:05 ampbas.canister_flux32
61425 Jun  7 23:42 ampbas.canister_flux33
61425 Jun  8 01:24 ampbas.canister_flux34
61425 Jun  6 10:44 ampbas.canister_flux4
61425 Jun  6 11:35 ampbas.canister_flux5
61425 Jun  6 12:31 ampbas.canister_flux6
61425 Jun  6 13:31 ampbas.canister_flux7
61425 Jun  6 14:12 ampbas.canister_flux8
61425 Jun  6 15:19 ampbas.canister_flux9
  111 Jun  6 07:26 ampbas.cg
  471 Jun  6 07:26 ampbas.covariance
1080243 Jun  8 10:38 ampbas.enp
  180 Jun  6 08:16 ampbas.expectation.1
  180 Jun  6 16:33 ampbas.expectation.10
  180 Jun  6 17:47 ampbas.expectation.11
  180 Jun  6 18:43 ampbas.expectation.12
  180 Jun  6 21:06 ampbas.expectation.13
  180 Jun  6 22:21 ampbas.expectation.14
  180 Jun  6 23:16 ampbas.expectation.15
  180 Jun  7 00:26 ampbas.expectation.16
  180 Jun  7 01:42 ampbas.expectation.17
  180 Jun  7 02:47 ampbas.expectation.18
  180 Jun  7 04:15 ampbas.expectation.19
  180 Jun  6 09:04 ampbas.expectation.2
  180 Jun  7 06:00 ampbas.expectation.20
  180 Jun  7 07:16 ampbas.expectation.21
  180 Jun  7 08:21 ampbas.expectation.22
  180 Jun  7 09:29 ampbas.expectation.23
  180 Jun  7 10:19 ampbas.expectation.24
  180 Jun  7 11:35 ampbas.expectation.25
  180 Jun  7 12:54 ampbas.expectation.26
  180 Jun  7 14:27 ampbas.expectation.27
  180 Jun  7 15:42 ampbas.expectation.28
  180 Jun  7 17:28 ampbas.expectation.29
  180 Jun  6 09:57 ampbas.expectation.3
  180 Jun  7 18:49 ampbas.expectation.30
  180 Jun  7 20:32 ampbas.expectation.31
  180 Jun  7 22:07 ampbas.expectation.32
  180 Jun  7 23:45 ampbas.expectation.33
  180 Jun  8 01:27 ampbas.expectation.34
  180 Jun  6 10:45 ampbas.expectation.4
```

```
  180 Jun  6 11:35 ampbas.expectation.5
  180 Jun  6 12:31 ampbas.expectation.6
  180 Jun  6 13:31 ampbas.expectation.7
  180 Jun  6 14:12 ampbas.expectation.8
  180 Jun  6 15:19 ampbas.expectation.9
 1597 Jun  6 07:26 ampbas.geom
 1015983 Jun  8 10:39 ampbas.hst
53804 Jun  6 07:17 ampbas.hyd
50805 May 25 10:03 ampbas.hyd.bak
50801 May 25 10:13 ampbas.hyd.tmp
 2152016 Jun  3 21:40 ampbas.ihead
  145 Jun  6 07:26 ampbas.krge_nbh
  110 Jun  6 07:26 ampbas.krige
  135 May 11 08:14 ampbas.parameters
  885 Jun  6 07:26 ampbas.presentation
 2936 Jun  6 07:26 ampbas.result_estimation
40006 Jun  6 07:26 ampbas.transport
11340 Jun  6 08:16 ampbas.travel_times1
11340 Jun  6 16:32 ampbas.travel_times10
11340 Jun  6 17:46 ampbas.travel_times11
11340 Jun  6 18:42 ampbas.travel_times12
11340 Jun  6 21:04 ampbas.travel_times13
11340 Jun  6 22:19 ampbas.travel_times14
11340 Jun  6 23:15 ampbas.travel_times15
11340 Jun  7 00:25 ampbas.travel_times16
11340 Jun  7 01:41 ampbas.travel_times17
11340 Jun  7 02:45 ampbas.travel_times18
11340 Jun  7 04:14 ampbas.travel_times19
11340 Jun  6 09:03 ampbas.travel_times2
11340 Jun  7 05:58 ampbas.travel_times20
11340 Jun  7 07:15 ampbas.travel_times21
11340 Jun  7 08:19 ampbas.travel_times22
11340 Jun  7 09:27 ampbas.travel_times23
11340 Jun  7 10:17 ampbas.travel_times24
11340 Jun  7 11:33 ampbas.travel_times25
11340 Jun  7 12:52 ampbas.travel_times26
11340 Jun  7 14:25 ampbas.travel_times27
11340 Jun  7 15:40 ampbas.travel_times28
11340 Jun  7 17:26 ampbas.travel_times29
11340 Jun  6 09:56 ampbas.travel_times3
11340 Jun  7 18:46 ampbas.travel_times30
```

```
11340 Jun  7 20:30 ampbas.travel_times31
11340 Jun  7 22:05 ampbas.travel_times32
11340 Jun  7 23:42 ampbas.travel_times33
11340 Jun  8 01:24 ampbas.travel_times34
11340 Jun  6 10:44 ampbas.travel_times4
11340 Jun  6 11:35 ampbas.travel_times5
11340 Jun  6 12:31 ampbas.travel_times6
11340 Jun  6 13:31 ampbas.travel_times7
11340 Jun  6 14:12 ampbas.travel_times8
11340 Jun  6 15:19 ampbas.travel_times9
13164 Jun  6 07:27 ampbas.trends
18394 Jun  8 10:34 bflux.dat
 7 May 11 08:38 casename.dsc
 1673954 Jun  6 08:15 conduc_1.dta.gz
  292 Jun  6 08:14 conduc_1.fld
 1674512 Jun  6 09:02 conduc_2.dta.gz
  292 Jun  6 09:02 conduc_2.fld
  739 Jun  8 10:34 efiler.dat
 1640114 Jun  6 08:15 head_1.dta.gz
  290 Jun  6 08:15 head_1.fld
 1635008 Jun  6 09:03 head_2.dta.gz
  290 Jun  6 09:02 head_2.fld
  640050 May 11 08:14 hypac.out
 2225386 Jun  7 18:45 lines.30
 2098811 Jun  7 20:28 lines.31
 2121221 Jun  7 22:04 lines.32
 2112672 Jun  7 23:42 lines.33
 2066773 Jun  8 01:23 lines.34
  363904 Jun  6 08:13 lines_1.hyp.gz
  319603 Jun  6 16:31 lines_10.hyp.gz
  319250 Jun  6 17:45 lines_11.hyp.gz
  373179 Jun  6 18:41 lines_12.hyp.gz
  315145 Jun  6 21:03 lines_13.hyp.gz
  339225 Jun  6 22:18 lines_14.hyp.gz
  340669 Jun  6 23:14 lines_15.hyp.gz
  338140 Jun  7 00:24 lines_16.hyp.gz
  309827 Jun  7 01:39 lines_17.hyp.gz
  324094 Jun  7 02:44 lines_18.hyp.gz
  357642 Jun  7 04:12 lines_19.hyp.gz
  318196 Jun  6 09:01 lines_2.hyp.gz
  363780 Jun  7 05:57 lines_20.hyp.gz
```

```
  328362 Jun  7 07:13 lines_21.hyp.gz
  347218 Jun  7 08:18 lines_22.hyp.gz
  334585 Jun  7 09:26 lines_23.hyp.gz
  326420 Jun  7 10:16 lines_24.hyp.gz
  328847 Jun  7 11:33 lines_25.hyp.gz
  330243 Jun  7 12:51 lines_26.hyp.gz
  346059 Jun  7 14:24 lines_27.hyp.gz
  338756 Jun  7 15:39 lines_28.hyp.gz
  339552 Jun  7 17:25 lines_29.hyp.gz
  335567 Jun  6 09:56 lines_3.hyp.gz
  348238 Jun  7 18:45 lines_30.hyp.gz
  329140 Jun  7 20:28 lines_31.hyp.gz
  332968 Jun  7 22:04 lines_32.hyp.gz
  330534 Jun  7 23:42 lines_33.hyp.gz
  318829 Jun  8 01:23 lines_34.hyp.gz
  341547 Jun  6 10:44 lines_4.hyp.gz
  324071 Jun  6 11:34 lines_5.hyp.gz
  348853 Jun  6 12:30 lines_6.hyp.gz
  311234 Jun  6 13:30 lines_7.hyp.gz
  350996 Jun  6 14:11 lines_8.hyp.gz
  357868 Jun  6 15:18 lines_9.hyp.gz
  776589 Jun  8 01:49 log.980606
   405 Jun  7 23:49 module.ini
62 Jun  6 07:22 pickts.ix
30 Jun  6 07:22 pickts.ts
 0 Jun  5 00:01 pickts.tsa
 2800 Jun  8 01:31 proper.lo
 2880 Jun  8 01:33 proper.loq
  152000 Jun  6 07:24 proper.ndx
 1095905 Jun  8 01:31 proper.st
 1043472 Jun  8 01:34 proper.sta
 1095905 Jun  8 01:33 proper.stq
  595 Jun  8 01:31 proper.te
  595 Jun  8 01:33 proper.teq
 0 Jun  8 01:33 proper.tl
80 Jun  8 01:33 proper.tlq
70 May 26 10:19 start*
78 May 11 08:14 submod.lib*
71115 May 13 09:47 system.dsc
```